

Numerical Study of Homogeneous and Heterogeneous Crystal Nucleation In Colloidal Systems

Dissertation
zur Erlangung des Grades
"Doktor der Naturwissenschaften"
am Fachbereich Physik
der Johannes Gutenberg-Universität Mainz

vorgelegt von
Hamed Maleki
geboren in Birjand (Iran)

Mainz, im Mai 2011

Zusammenfassung

Im Rahmen dieser Arbeit wurden Computersimulationen von Keimbildungs- und Kristallisationsprozessen in kolloidalen Systemen durchgeführt. Eine Kombination von Monte-Carlo-Simulationsmethoden und der Forward-Flux-Sampling-Technik wurde implementiert, um die homogene und heterogene Nukleation von Kristallen monodisperser Hartkugeln zu untersuchen. Im mäßig unterkühlten Bulk-Hartkugelsystem sagen wir die homogenen Nukleationsraten voraus und vergleichen die Resultate mit anderen theoretischen Ergebnissen und experimentellen Daten. Weiterhin analysieren wir die kristallinen Cluster in den Keimbildungs- und Wachstumszonen, wobei sich herausstellt, dass kristalline Cluster sich in unterschiedlichen Formen im System bilden. Kleine Cluster sind eher länglich in eine beliebige Richtung ausgedehnt, während größere Cluster kompakter und von ellipsoidaler Gestalt sind.

Im nächsten Teil untersuchen wir die heterogene Keimbildung an strukturierten bcc (100)-Wänden. Die 2d-Analyse der kristallinen Schichten an der Wand zeigt, dass die Struktur der Wand eine entscheidende Rolle in der Kristallisation von Hartkugellkolloiden spielt. Wir sagen zudem die heterogenen Kristallbildungsraten bei verschiedenen Übersättigungsgraden voraus. Durch Analyse der größten Cluster an der Wand schätzen wir zusätzlich den Kontaktwinkel zwischen Kristallcluster und Wand ab. Es stellt sich heraus, dass wir in solchen Systemen weit von der Benetzungsregion entfernt sind und der Kristallisationsprozess durch heterogene Nukleation stattfindet.

Im letzten Teil der Arbeit betrachten wir die Kristallisation von Lennard-Jones-Kolloidsystemen zwischen zwei ebenen Wänden. Um die Erstarrungsprozesse für ein solches System zu untersuchen, haben wir eine Analyse des Ordnungsparameters für die Bindung-Ausrichtung in den Schichten durchgeführt. Die Ergebnisse zeigen, dass innerhalb einer Schicht keine hexatische Ordnung besteht, welche auf einen Kosterlitz-Thouless-Schmelzvorgang hinweisen würde. Die Hysterese in den Erhitzungs-Gefrierkurven zeigt darüber hinaus, dass der Kristallisationsprozess einen aktivierten Prozess darstellt.

Abstract

In this thesis we have performed computer simulations of nucleation and crystallization in colloidal systems. Monte Carlo simulation method combined with forward flux sampling technique is implemented to study homogeneous and heterogeneous crystal nucleation of monodisperse hard spheres. In the moderate super-cooling of bulk hard sphere system, we predicted the homogeneous nucleation rates and compared the results with other theoretical results and experimental data. We also analyze the crystalline clusters in the nucleation and growth regions. We found that crystalline clusters in the system formed in different shapes. Small clusters are more elongated in one arbitrary direction, however, bigger clusters are more compact and have an ellipsoidal shape.

In the next part, we studied heterogeneous nucleation at the structured bcc (100) wall. $2d$ analysis of crystalline layers at the wall showed that the structure of the wall has a crucial role in solidification of hard sphere colloids. We also predicted heterogeneous crystal nucleation rates for different degrees of supersaturation. Additionally, by analyzing of the largest clusters at the wall, we estimated the contact angles between crystalline clusters and the wall. We found that for such system, we are far from wetting region and crystallization process happens via heterogeneous nucleation.

In the last part of the thesis, we reported the crystallization of Lennard-Jones colloidal system confined between two planar walls. In order to study freezing process for such system, we performed the bond-orientational order parameter analysis in the layers. The results showed that there is no hexatic order inside the layer which would indicate the Kosterlitz-Thouless melting process. Also the hysteresis in the heating-freezing curves shows that the crystallization process proceeds an activated process.

Contents

1	Introduction	1
1.1	Overview	3
2	Methods	5
2.1	Phase transitions and the nucleation phenomenon	6
2.2	Classical theory of nucleation	8
2.2.1	Classical theory of nucleation and the free energy barrier	9
2.2.2	Cluster size distribution	12
2.2.3	Classical nucleation theory of the nucleation rate	13
2.3	Rare events simulation methods	15
2.3.1	Forward flux sampling	17
2.4	Identification of crystalline clusters: Local bond order parameter	21
3	Determination of crystal nucleation rates of hard sphere suspensions	25
3.1	Introduction	26
3.2	Computational methodology and simulation strategies	27
3.3	Results and discussion	30
3.4	Conclusion	39
4	Heterogeneous nucleation of hard sphere system at the hard wall	41
4.1	Introduction	42
4.2	Computational methodology and details	43
4.3	Results and discussion	44
4.3.1	2D analysis	44
4.4	Conclusion	53
5	2D versus 3D Freezing of a Lennard-Jones Fluid in a Slit Pore	55
5.1	Introduction and background	56
5.2	Simulation method	57
5.3	Results and discussion	58
5.4	Conclusion	66
6	Summary and outlook	69

List of Figures	72
List of Tables	73
Bibliography	82

1 Introduction

Vapor, liquid and ice are three different equilibrium phases of water in nature. Pure water normally evaporates at $100^{\circ}C$ and freezes at $0^{\circ}C$. However, it can also be "supercooled" at the standard pressure down to almost $-42^{\circ}C$ without freezing. Supercooling, also known as under-cooling [1, 2], is the process of lowering the temperature of a liquid or a gas below its freezing points without it becoming a solid. A liquid below its standard freezing point will crystallize in the presence of a seed crystal, a nucleus around which a crystal structure can form or at a wall of container. However, lacking any such nucleus or external effects, the liquid phase can be maintained all the way down to the temperature at which crystal homogeneous nucleation occurs (In the supercooled metastable state).

Crystal nucleation is an example of transformation at the first order phase transition. The same phenomenon happens if the starting system is a superheated liquid, triggering in to the vapor. Nucleation is also a rare event happening in the nature. In rare events, the average waiting time between events can be several order of magnitude longer than the event time itself and as a consequence, rare events are basically difficult to study and investigate. However, nucleation has many practical consequences in science and technology. In materials science, the casting of metals gives physical properties that depend on the conditions of crystal growth. If large under-coolings can be achieved before nucleation occurs (as in the rapid solidification processing) different and potentially useful forms of the metals may be produced. In atmospheric sciences, the nucleation of both water droplets and ice crystals in the atmosphere has a major effect both short-term on the weather and long-term through global warming (or cooling) by cloud formation.

Fahrenheit was the first who studied the crystallization of water [1], by the concept of supercooling. Later Gibbs gave a detailed description of the criteria for the phase equilibria [3]. He suggested the distinction between stable, metastable and unstable phases, to understand the phase transformation from the metastable phase to the stable phase. Volmer and Weber [4] were the first scientist who formulated a theory of nucleation, the so called "classical nucleation theory" (CNT). Classical theory of nucleation is the best qualitatively understood framework of nucleation phenomena. In CNT, the free energy of spherical nuclei contains both surface and bulk terms. The surface term describes the free energy needed to create an interface between solid and liquid phases. This

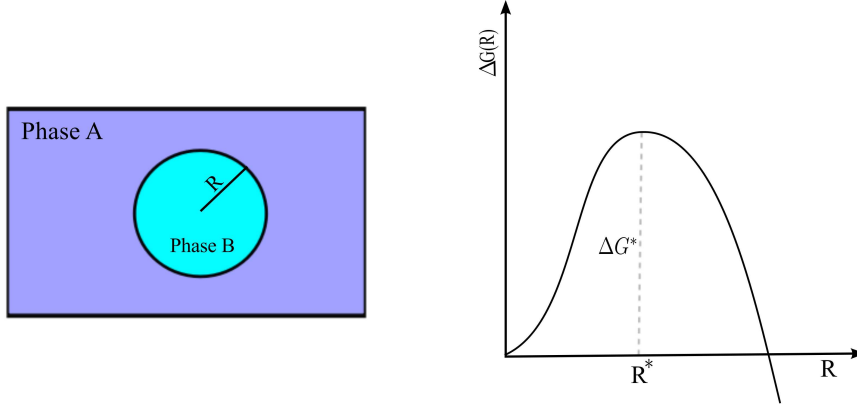


Figure 1.1: Snapshots of the spherical solid cluster radius R in the metastable liquid phase (left-hand side). Also the Gibbs free energy barrier of nuclei, as a function of R .

term is positive and proportional to the area of the liquid-solid interface. The bulk term takes care of the fact that the solid phase is more stable than the liquid phase. This term is negative and proportional to the volume of the solid cluster. According to classical nucleation theory, the Gibbs free energy of a solid spherical nucleus of radius R is written as

$$\Delta G = 4\pi R^2 \gamma + \frac{4}{3}\pi R^3 \rho_s \Delta\mu , \quad (1.1)$$

where ρ_s is the number density of the bulk solid, $\Delta\mu$ the difference in chemical potential between the liquid and the solid (negative value), and γ is the liquid-solid surface free energy density.

ΔG as a function of nucleus radius R , has a maximum at $R^* = 2\gamma/(\rho|\Delta\mu|)$ and the critical height of the nucleation barrier is given by

$$\Delta G^* = \frac{16\pi}{3} \frac{\gamma^3}{(\rho_s |\Delta\mu|)^2} . \quad (1.2)$$

Figure 1.1 shows the behavior of the Gibbs free energy barrier of a solid cluster, as a function of radius R . The probability of the formation of the critical cluster depends exponentially on its free energy and has the form of

$$P^* \propto e^{-\beta \Delta G^*} , \quad (1.3)$$

where $\beta = 1/k_B T$.

The rate of nucleation in CNT is given by the product of P^* and a kinetic factor k .

The expression for nucleation rate from CNT is

$$Rate = k e^{-\frac{16\pi}{3k_B T} \frac{\gamma^3}{(\rho_s |\Delta\mu|)^2}} \quad (1.4)$$

with $k = 24\rho_l Z D_s n^{*2/3} / \lambda^2$. here ρ_l is the number density of the liquid, $Z = \sqrt{|\Delta\mu| / 6\pi k_B T n^*}$ is the Zeldovich factor, D_s is the self-diffusion coefficient, n^* is the critical nucleus size, and λ is the typical diffusion distance for particles to attach to the critical nuclei.

Nowadays, CNT is the most used theory to understand the nucleation processes from experimental and numerical measurements. In this thesis we attempt to study homogeneous and heterogeneous nucleation phenomena using numerical techniques to simulate the crystal nucleation process. we use forward flux sampling (FFS) in combination with the local bond-order analysis for identification of the crystal nuclei, to predict crystal nucleation rates for homogeneous and heterogeneous systems. In addition, we analyze the size and the shape of clusters in different trajectories and pathways.

1.1 Overview

In this thesis we study the numerical investigation of homogeneous and heterogeneous nucleation in hard sphere colloidal systems. Forward flux sampling (FFS) technique [5, 6, 7, 8, 9] is applied to predict crystal nucleation rates. Additionally, we used local bond-order analysis for the identification of critical nuclei and to study the structure of critical nuclei. We also study the solidification of Lennard-Jones system confined in a slit pore as a first step for studying heterogeneous crystal nucleation in such system. This thesis is organized as follows:

In chapter I, we discuss detailed homogeneous classical nucleation theory (*CNT*). Here we review an expression for free-energy barriers and also nucleation rates. Then we present the numerical and computational techniques used in the thesis: Forward flux sampling (FFS) in order to predict nucleation rate constants and to analyze the nucleation pathways during process. Before describing FFS in more details, we have a short review about other computational methods as a history of FFS to study rare events.

In chapter II, we study homogeneous crystal nucleation for hard sphere colloidal systems using forward flux sampling. We predict nucleation rates in moderate undercooling and compare them with the umbrella sampling (US) method [10, 11, 12] of Auer and Frenkel [13], brute force molecular dynamics and Monte Carlo simulations [14, 15] and experimental data [16, 17, 18]. We also apply the tensor of gyration in colloidal model to analyze crystal clusters in the hard sphere system and in different pathways for different pressures.

In chapter III, we develop FFS to study heterogeneous crystal nucleation of hard spheres confined between one bcc(100) structured wall and one planar repulsive wall. The aim of this chapter is to study the effect of structured wall on crystal nucleation. In this part, for the first time we predict heterogeneous nucleation rates of hard sphere and analyze the critical clusters at the bcc-wall by means of the gyration tensor.

Finally in chapter IV we apply standard molecular dynamics (MD) simulation techniques to study solidification of the Lennard-Jones colloidal system confined in a slit pore. In this system we are interested to see if hexatic order which would indicate a melting scenario of the Kosterlitz-Thouless type is occurring in the system. For this system we did some 2D analysis and also we study the dynamics of the system by computing diffusion coefficients.

2 Methods

In this chapter we explain a physical description of phase transitions and in particular the nucleation phenomenon. We start with phase transitions and different phases in the nature. Next we describe nucleation phenomena and continue with derivation of the classical theory of nucleation and CNT expression for nucleation rates and free energy barriers. In the next part, we review numerical tools which are needed to study rare events and the forward flux sampling (FFS) technique used in this thesis. Finally, at the end of the chapter, we define the bond order parameter and the reaction coordinate to identify solid-like particles and also identification of the cluster used in numerical simulations of nucleation.

2.1 Phase transitions and the nucleation phenomenon

Nucleation phenomenon is an example of the first order phase transition in the nature [19]. The condensation of gases, melting of solids, freezing of liquids and etc., are examples of thermodynamic first order phase transitions in daily life. These phenomena are classified as first order phase transitions, because they involve a discontinuous change in the density ρ , which corresponds to the first derivative of the Gibbs free energy per particle (the chemical potential μ) with respect to the pressure (P) at the constant temperature T . Gibbs was the first to study the liquid to the vapor phase transition between two phases [3]. Figure 2.1 shows an isotherm curve of a simple fluid in the $P - V$ plane, also corresponding diagram of the free energy.

In general phase transition can be considered as a quantitative variable of the structure or the reaction of a physical system with respect to a change of external parameters like pressure, temperature, electric and magnetic fields. A phase transition occurs when a phase becomes unstable in the given thermodynamic conditions described with intensive variables (P, T, \dots). During such a phase transition, the physical system may transfer from the stable state to an intermediate state called "metastable" equilibrium state which is a thermodynamic state intermediate between stable and unstable states. Liquid water at the temperature below 0°C typically corresponds to a meta-stable state named "super-cooled" water. Similarly, a substance maintained in a liquid state above its boiling point is also in a metastable state called "super-heated".

In principle, when a material undergoes a transformation from an initial stable equilibrium state, it passes from metastable state to instability and then a phase transition is observed. The thermodynamic description of phase transitions says nothing about the evolution of the phase in time nor about the kinetics of the transition phenomenon. For instance, phase diagrams only give information about the coexistence of phases (as a function of pressure, temperature, concentration, etc.) and not the time required for passing from one phase to another one, when thermodynamic parameters of a system are changed. So far know that the phase change is not instantaneous and that it is a dynamic phenomenon and each transition has its own kinetics. The dynamic description of the phase transition implies that the mechanism of transformations are known in advance and they are very varied. The most frequently involves the formation of micro structures which are the "nuclei" of the new phase that appears during the transformation: this is called the nucleation phenomenon. For example, nucleation is encountered in a liquid during crystallization when crystallites, the nuclei of the solid phase are formed.

When a liquid is under-cooled, the solid is more stable than the liquid. However, the liquid will not crystallize immediately. First, nuclei of the solid phase have to be formed. This is an activated process. The nucleus has to cross a free-energy barrier in

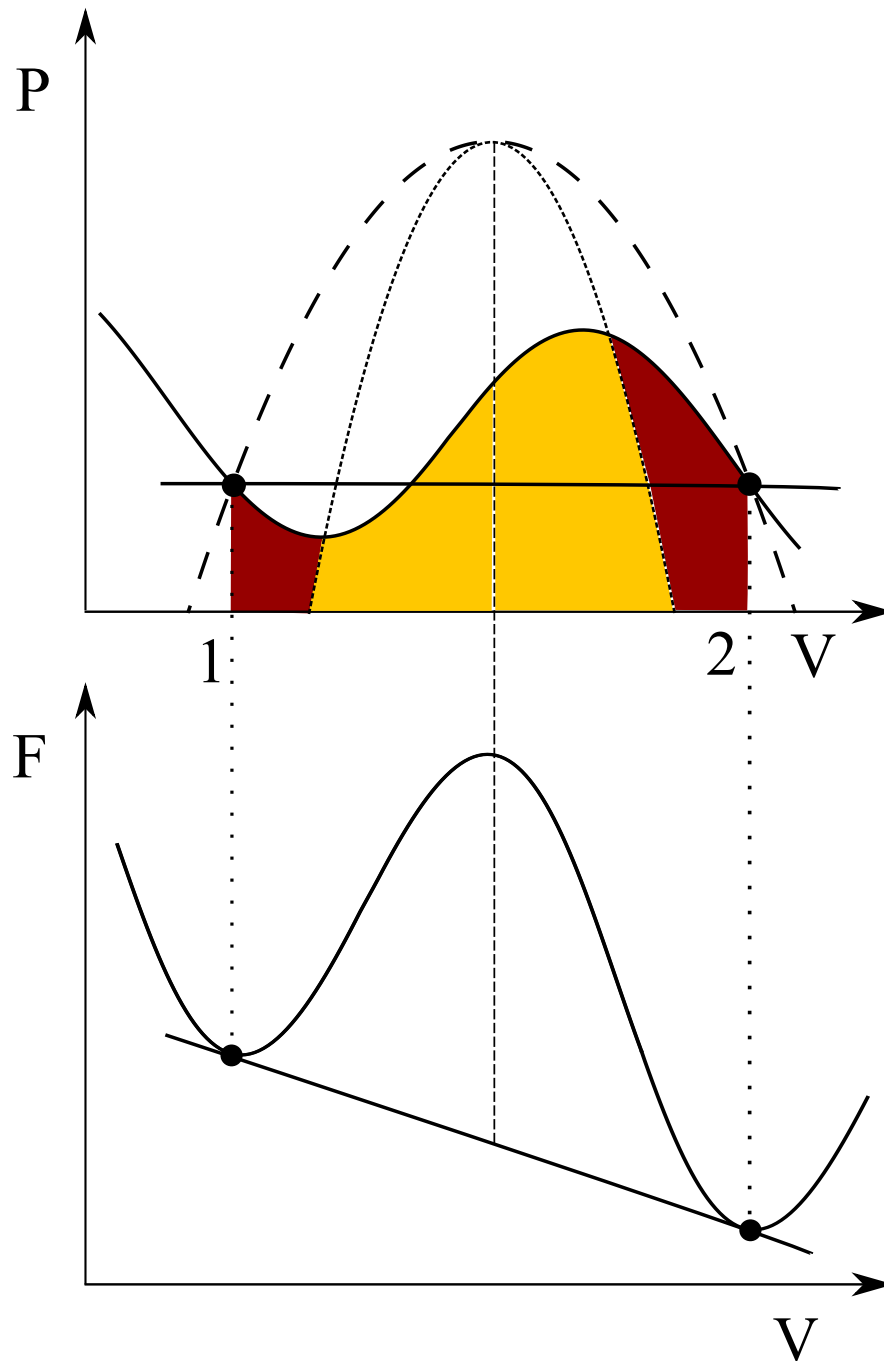


Figure 2.1: Pressure-Volume and Free-energy-Volume of simple fluid in constant temperature T . Filled circles in $P - V$ curve are correspond to the coexistence pressure between two given phases i. e. the vapor and liquid phases.

order to grow into a bulk crystal. Nuclei at the top of the free-energy barrier are called critical nuclei. Nuclei that are smaller than the critical nucleus size, the so-called pre-critical nuclei, have a tendency to shrink, because in that way they can lower their free energy. For the same reason, nuclei that are larger than the critical size, the so-called post-critical nuclei, tend to grow.

In this case nucleation is only possible if atoms or molecules constituting the material, can diffuse within it to aggregate and thus form the nuclei of the new phase. Diffusion is then the key mechanism that guides the nucleation phenomenon itself and determines its kinetics. The interfacial properties, particularly the interfacial free energy, also play an important role in nucleation and the appearance of the nucleus of the new phase and creation of an interface between two phases. Also external objects and effects like surfaces and dust particles in the system change the process of nucleation in such a phase transition.

Depending on the role of foreign bodies and external effects, nucleation phenomena can be either homogeneous or heterogeneous. In the first case the energy barrier that a system must overcome to generate crystal nuclei (from a homogeneous mother phase) depends on geometrical parameters, on temperature, supersaturation and on the specific energy of the interface between the mother phase and that crystallising from it. Therefore, in homogeneous nucleation due to spontaneous density fluctuations in the bulk of a pure phase, transition happen. In the second case (when other bodies exist in the system) new interfaces must be considered which exert an additional influence on the activation barrier for nucleation and hence on the nucleation rate. Here the phase transition can be assisted by walls or impurities within the system. Clusters on the new phase are also formed at the surface of these foreign bodies. Figure 2.2 shows two experimental examples of homogeneous and heterogeneous nucleation.

2.2 Classical theory of nucleation

Classical nucleation theory (CNT) is the most common theory to describe the nucleation phenomenon. This theory is employed to predict the nucleation rates and estimate the nucleation barrier. Starting point of the theory formulated by Volmer and Weber [4] and extended by Farkas [20], Becker and Döring [21], and Turnbull and Fisher [2]. Volmer and Weber applied the Gibbs formulation of the reversible work of a new stable phase happening in a metastable parent phase. This was a first theory of nucleation which would calculate the nucleation rate. Later on, Farkas formulated a kinetic model cluster evolution. Afterwards, Becker and Döring argued that a steady-state distribution was more suitable than the equilibrium distribution proposed by Volmer and Weber, and obtained an expression for a steady-state nucleation rate in a vapour condensation experiment.

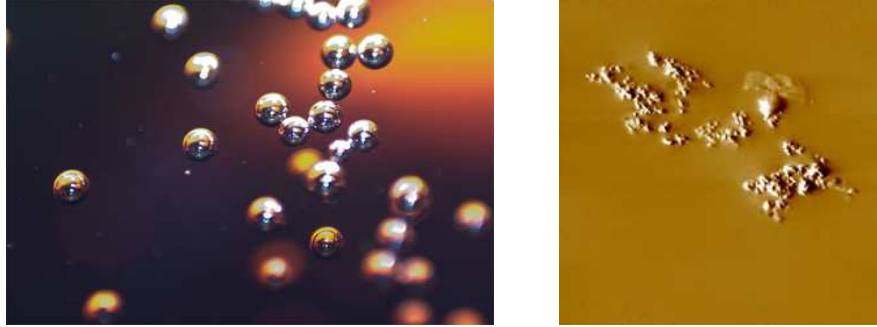


Figure 2.2: On the right-side: an experimental example of heterogeneous crystal nucleation and growth. This AFM tapping/phase mode image shows the nucleation of a poly(lactide) spherulite in the melt at 95°C. The nucleation is heterogeneous, i.e. the growth starts at impurities like dust particles. Schematic three-dimensional representation of a particle surrounded by its neighbors (courtesy of Ralf Thomann (Freiburg Materials Research Center)). On the left-side: bubbles in a soft drink each nucleate independently, responding to a decrease in pressure (Photos courtesy of Wikipedia).

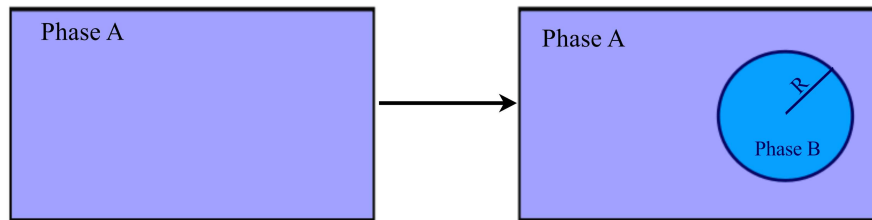


Figure 2.3: Schematic formation of nucleus of the new stable phase B in a meta-stable parent phase A . The nucleation barrier is given by the free energy difference of the two systems.

In the following we review the CNT derivation of the reversible work for the formation of a cluster in a metastable phase and define the equilibrium distribution of cluster sizes and also the nucleation rate.

2.2.1 Classical theory of nucleation and the free energy barrier

In this section we describe the classical nucleation theory of the free energy barrier and the equilibrium size distribution of clusters. As a start point we assumed a system in a metastable phase A , for instance a vapor (left-hand side of Fig. 2.3), at thermodynamic conditions where the stable phase B (for instance liquid) exists. Phase B after reaching the critical size starts growing in the parent phase A (right side in Fig. 2.3).

To facilitate relations, we label the initial metastable phase A (left-hand side of Fig. 2.3) as a system I and system II is the metastable phase A when a stable phase

B exists (on the right-hand side in Fig. 2.3). The aim is to compute the reversible work for the formation of a cluster of the new stable phase B in the parent phase A at constant temperature and pressure. For this reason, first we calculate the internal energy of the system in both situations I and II. In system I which is containing only the A phase, the internal energy is

$$U_A^I = S^I T^I - P^I V + \mu^I N, \quad (2.1)$$

where S is the total entropy of the system, T the absolute temperature, P the pressure, V the total volume, μ the chemical potential and $N = N_A$ is the total number of particles. In system II, the internal energy is

$$U_{A+B}^{II} = S^{II} T^{II} - P_A^{II} V_A^{II} - P_B^{II} V_B^{II} + \gamma \mathbf{A} + \mu_A^{II} N_A + \mu_B^{II} N_B, \quad (2.2)$$

where P_A and P_B are the pressures of phase A and B respectively, V_A and V_B their volumes, γ the interfacial free energy existing between two phases, \mathbf{A} the surface area of the stable state B , μ_A and μ_B their chemical potential N_A and N_B the number of particles in A and B phases.

We assume the temperature throughout the system is uniform ($T^I = T^{II}$), but no uniformity of the pressure or the chemical potential yet required. The total number of particles in the system is given by $N = N_A + N_B$ and the total volume $V = V_A + V_B$. Therefore, Eq. 2.2 can be written as

$$U_{A+B}^{II} = T^{II} S^{II} - P_A^{II} V + (P_A^{II} - P_B^{II}) V_B^{II} + \gamma \mathbf{A} + \mu_A^{II} N + (\mu_B^{II} - \mu_A^{II}) N_B. \quad (2.3)$$

As the system is in constant pressure, $P = P^I = P_A^{II}$ and also since $N_A \gg N_B$, $\mu^I = \mu_A^{II}$. The reversible work to grow a cluster of phase B from the parent phase A is obtained by the Gibbs free energy difference between situations I and II. We define the Gibbs free energy of the system I by G_A^I and in system II by $G = G_{A+B}^{II}$. As the system is in constant-pressure, constant-temperature (NPT), the Gibbs free energy difference is define as

$$\Delta G = \Delta U + P \Delta V - T \Delta S. \quad (2.4)$$

Thus, by using this equation and also Eqs. 2.1 and 2.3, ΔG can be written as

$$\Delta G = G_{A+B}^{II} - G_A^I = (P - P_B^{II}) V_B^{II} + \gamma \mathbf{A} + (\mu_B^{II} - \mu_A^{II}) N_B \quad (2.5)$$

where $\mu_A^{II} = \mu_A^{II}(P_A)$ and $\mu_B^{II} = \mu_B^{II}(P_B)$.

The final expression of the nucleation free energy in CNT is obtained with a few assumptions. First, the growing clusters are characterized by the bulk properties of the stable phase B . The cluster in phase B has a spherical shape and the interfacial

free energy γ is also independent from the radius of the cluster, and therefore $\gamma = \gamma_\infty$, that γ_∞ is the interfacial free energy of a sphere with an infinite radius, i.e. a flat interface. Last assumption is about incompressibility of clusters. The cluster in phase B is incompressible and its density ρ does not change with pressure. Also in thermodynamics, we know that, at constant temperature

$$\frac{d\mu}{dP} = \frac{V}{N} = \rho^{-1}. \quad (2.6)$$

Thus the chemical potential of the new phase b can be written as

$$\mu_B^{II}(P_B^{II}) = \mu_B^{II}(P_A^{II}) + \frac{P_B^{II} - P_A^{II}}{\rho_B} \quad (2.7)$$

where ρ_B is the density of phase B .

By using CNT assumptions and also Eq. 2.7, the expression for the free energy of a cluster with area \mathbf{A} containing N_B particles in parent phase A is

$$\begin{aligned} \Delta G(N_B) &= \gamma_\infty \mathbf{A}(N_B) + [\mu_B^{II}(P_A) - \mu_A^{II}(P_A)]N_B \\ &= \gamma_\infty \mathbf{A}(N_B) - |\Delta\mu|N_B \end{aligned} \quad (2.8)$$

where $|\Delta\mu|[\mu_B^{II}(P_A) - \mu_A^{II}(P_A)]$ is the chemical potential difference between two phases and is a negative quantity, and \mathbf{A} depends on the cluster shape which is a spherical shape due to CNT assumptions. Hence the area of cluster is $\mathbf{A} = 4\pi R^2$ and also $V_B = \frac{4}{3}\pi R^3$ and $\rho_B = N_B/V_B$. Finally the Gibbs free energy of formation of a spherical cluster of phase B with radius R in the metastable phase A is

$$\Delta G(R) = 4\pi R^2 \gamma_\infty - |\Delta\mu| \rho_B \frac{4}{3}\pi R^3 \quad (2.9)$$

According to Eq. 2.9, the Gibbs free energy difference contains two terms, the surface term and the volume term. The first term is the surface term which is the free energy cost for creating an interface between phases A and B . This term is positive and proportional to the surface area of the cluster and called the surface free energy. The second term is a bulk term which is negative and proportional to the volume of the cluster in the system and is called volume free energy. This term expresses the fact that the phase B is more stable than the parent phase A . Figure 2.4 shows the behavior of the Gibbs free energy versus the radius of the cluster. The function ΔG goes through a maximum value at

$$R^* = \frac{2\gamma_\infty}{|\Delta\mu|\rho_B} \quad (2.10)$$

which denotes the critical cluster size. For small clusters, the surface term dominates and the free energy increases, however, if this nucleus exceeds the critical size, the

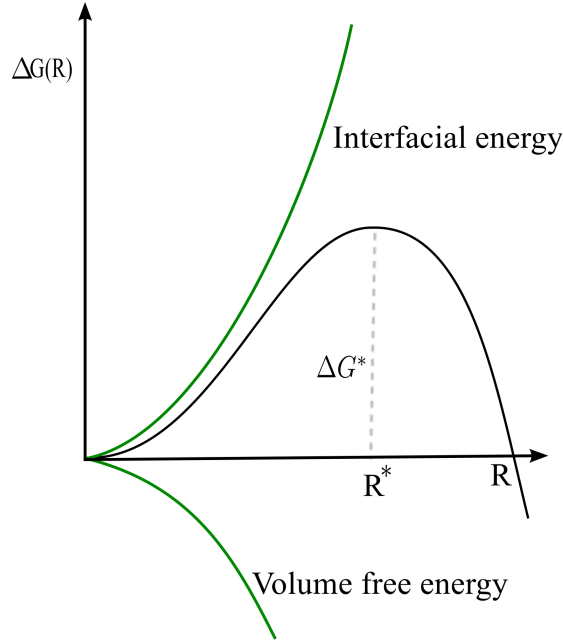


Figure 2.4: Classical nucleation theory prediction of Gibbs free-energy of a cluster as a function of its radius R .

volume free energy term dominates, its free energy decreases and stable phase B starts to grow. The corresponding height of the free energy barrier of nucleation is then

$$\Delta G^* = \frac{16\pi}{3} \frac{\gamma_\infty^3}{(|\Delta\mu|\rho_B)^2}. \quad (2.11)$$

2.2.2 Cluster size distribution

By using Eq. 2.8 (The Gibbs free energy difference between two situations I and II at constant temperature) and defining $N_B = n$, we can introduce the chemical potential of a cluster of size n as

$$\mu_n(P) = \gamma\mathbf{A} + n\mu_B(P) \quad (2.12)$$

where P is the pressure of phase A . In order to compute the equilibrium distribution of clusters, we assume a low concentration of clusters forming in the metastable phase A and a cluster size n exerts a partial pressure P_n on the system (such as $\sum_{i=1}^{\infty} P_i = P$). Thus the chemical potential of a cluster size n at P_n is

$$\mu_n(P_n) = \mu_n(P) + k_B T \ln\left(\frac{P_n}{P}\right). \quad (2.13)$$

In this equation, we used $d\mu/dP = 1/\rho$ and the ideal gas equation of state ($P = \rho k_B T$). By using Eq. 2.13, it is possible to rewrite Eq. 2.8 as

$$\Delta G = \mu_n(P_n) - k_B T \ln\left(\frac{P_n}{P}\right) - n\mu_A(P). \quad (2.14)$$

By using the fact that at equilibrium, $\mu_n P_n = n\mu_A(P)$, the free energy barrier expression in CNT becomes

$$\Delta G = -k_B T \ln\left(\frac{P_n}{P}\right). \quad (2.15)$$

Also by means of Raoult's law, P_n/P is equal to $N_n/N_A \sim N_n/N$, the CNT expression of the equilibrium distribution for clusters of size n is

$$\Delta G = -k_B T \ln\left(\frac{N_n}{N}\right) = -k_B T \ln(P(n)), \quad (2.16)$$

where $P(n)$ is the probability to have a cluster of size n .

2.2.3 Classical nucleation theory of the nucleation rate

Calculating a nucleation rate was first formulated by Volmer and Weber [4]. Classical nucleation theory attempts to understand the kinetics of the nucleation process of clusters of the new phase (called phase B) from the metastable initial phase A , by computing the nucleation rate. This theory assumes that clusters of the phase B slowly grow or shrink via the attachment of single particles:



where B_{n-1} is a cluster with $n - 1$ particles, B_1 with one particle, $k_{+,n-1}$ the attachment rate of one monomer to the B_{n-1} cluster, and $k_{-,n}$ the detachment rate. This assumption was initially made for vapour-liquid nucleation, where the concentration of monomers is much larger than the one of dimers and where collisions between growing clusters are extremely rare [22]. By solving the following master equation, we compute the time dependent cluster distribution $N_n(t)$.

$$\frac{dN_n(t)}{dt} = N_{n-1}(t)k_{+,n-1} - [N_n(t)k_{-,n} + N_n(t)k_{+,n}] + N_{n+1}(t)k_{-,n+1}. \quad (2.18)$$

The nucleation rate at a given cluster size n is a time dependent flux of clusters that reaches n , and is given by

$$R_{n,t} = N_n(t)k_{+,n} - N_{n+1}(t)k_{-,n+1}. \quad (2.19)$$

To obtain the rate in this equation, two assumptions are needed. First, when the clusters in the system are larger than the critical cluster, the back flux is zero ($N(t) = 0$ for $n > n^*$). The second assumption is for $n < n^*$, $N(t)$ is the equilibrium clusters distribution N_n with $N \sim N_1$ the total number of monomers and $e^{-\beta\Delta G(n^*)}$ determines the probability to find the critical cluster n^* . Therefore eq. 2.19 has become

$$R = N_n k_{+,n^*} = N_1 k_{*,n^*} e^{-\beta\Delta G(n^*)} \quad (2.20)$$

where k_{+,n^*} is the attachment rate of a single particle to the critical cluster, and $\Delta G(n^*)$ is the free energy barrier to nucleation.

Becker and Döring replaced the equilibrium clusters distribution N_n with a steady-state clusters distribution N_n^s , and changed eq. 2.19 into

$$R = N_n^s k_{+,n} - N_{n+1}^s k_{-,n-1}, \quad (2.21)$$

an equation that can be solved by recurrence (see e.g. Ref. [23])

$$R = N_1 \left[\sum_{i=1}^{\infty} \frac{1}{k_{+,n} \xi_n} \right]^{-1} \quad (2.22)$$

where

$$\xi_n = \prod_{j=1}^{n-1} \frac{k_{+,n}}{k_{-,n+1}} \quad \text{for } n > 1. \quad (2.23)$$

To explicitly determine R , it is assumed that the rate constant does not depend on the system being in equilibrium. Imposing the system initially in equilibrium,

$$n N_1 \overset{K}{\rightleftharpoons} N_n \quad (2.24)$$

where N_1 is the equilibrium distribution of monomers, N_n the equilibrium distribution of clusters of size n , and K the equilibrium constant and relate the ratio of rate constants $\frac{k_{+,n}}{k_{-,n+1}}$ in the eq. 2.23 to the equilibrium constant. The equilibrium constant K for this reaction is then given by eq. 2.16, and thus eq. 2.22 becomes

$$R = N_1 \left[\sum_{i=1}^{\infty} \frac{1}{k_{+,n} e^{-\beta\Delta G(n)}} \right]^{-1}. \quad (2.25)$$

Becker and Döring used several approximation in order to compute the nucleation rate R . First, near the top of the free-energy barrier, $\delta G(n^*)$ dominates the sum in eq. 2.25. Next assumption is, $\delta G(n)$ is replaced by the first two non-zero terms of the Taylor expansion around n^* , and $k_{+,n}$ is replaced by k_{+,n^*} . Finally, the sum is replaced by an integral from $n - n^* = -\infty$ to $n - n^* = \infty$, considering N_n to be the continuous

function of n . By these approximations, the final expression of the nucleation rate is:

$$R = N_1 k_{+,n^*} \left(\frac{|\Delta G''(n)|_{n^*}}{2\pi k_B T} \right)^{1/2} e^{-\beta \Delta G(n^*)}, \quad (2.26)$$

where $|\Delta G''(n)|_{n^*}$ is the second derivative of the Gibbs free energy $\Delta G(n)$ with respect to n computed at the critical cluster size n^* , and

$$Z = \left(\frac{|\Delta G''(n)|_{n^*}}{2\pi k_B T} \right)^{1/2} \quad (2.27)$$

is the Zeldovitch factor [24].

By using the expression of ΔG as a function of n in CNT, we can write the nucleation rate per unit volume as

$$R = N_1 k_{+,n^*} \left(\frac{|\Delta \mu|}{6\pi k_B T n^*} \right)^{1/2} e^{-\beta \Delta G(n^*)}. \quad (2.28)$$

where

$$Z = \left(\frac{|\Delta \mu|}{6\pi k_B T n^*} \right)^{1/2}. \quad (2.29)$$

By defining κ as a kinetic pre-factor, eq. 2.29 can be written as

$$R = \kappa e^{-\beta \Delta G(n^*)}, \quad (2.30)$$

where

$$\kappa = N_1 k_{+,n^*} Z. \quad (2.31)$$

It is clear that by increasing the super saturation ($\Delta \mu$), the nucleation rate R increases.

2.3 Rare events simulation methods

Simulation of first order phase transition phenomena like nucleation is difficult to investigate. The free energy barrier which separates the metastable phase from stable phase causes nucleation to become a rare event. In conventional (brute-force) simulations, the system will usually fluctuate around its metastable free energy minimum. To study nucleation by using normal simulations on a reasonable time-scale and on the small length scales, we have to impose an extreme supersaturation to the system. If we are interested to reduce the supersaturation applied to the system, the free energy barrier gets higher and the probability to detect the nucleation event on such time and length scales gets extremely low. In this situation, the system spends a long time in a stable state and rarely jumps to another state in a short time. Therefore, the study of nucleation event requires advanced sampling methods.

The separation of time scales (waiting time to observe a nucleation event and the time that nucleation itself takes) makes it possible to describe the kinetics of rare events as a product of two factors: the probability of reaching the top of the free energy barrier and the rate at which it is crossed. The initial idea in this approach was contained in transition state theory (TST) [25, 26]. The first step in this approach is the definition of a reaction coordinate Q and its description that measures the progress of the transition from one metastable phase to the final stable phase. For $Q < Q^*$, the system is in the domain of attraction of state A , and for $Q > Q^*$ the system likes to grow and reaches the final state B . The transition surface is formed by the set of all points in configuration space where the probability to reach states A or B is 0.5. The surface $Q = Q^*$ provides an approximation to the transition state.

When we know the location of the transition state in phase space, it is then possible to formulate the rate of the rare event like nucleation. This computation involves two major steps. In the first step we compute the reversible work $\Delta W(Q)$ required to move the system from the A metastable state to the transition state (at Q^*). The probability that spontaneous equilibrium fluctuations bring the system to the transition state is

$$P(Q^*) = e^{-\beta W(Q^*)}, \quad (2.32)$$

where β is $1/k_B T$. As we showed in the classical nucleation theory of the free energy barrier, the reversible work to nucleate a new stable phase from the metastable parent phase with size Q^* is proportional to the Gibbs free energy ΔG . Therefore we have

$$P(Q^*) = e^{-\beta \Delta G(Q^*)}. \quad (2.33)$$

As a next step, since the system is at the transition state, it is possible to calculate the frequency of successful crossings of trajectories started from the transition state. This term gives us the crossing rate $k(Q^*)$. The product of these two steps give an expression for the rate of the rare events:

$$R = k(Q^*)P(Q^*). \quad (2.34)$$

In the last twenty years, several algorithms were developed to study rare events. Bennett-Chandler method is one of the first algorithms which is based on this two-step procedure [26]. In this method, $P(Q^*)$ can be computed by means of the Umbrella Sampling (US) technique [12, 10]. Disadvantages of this method are that it is computationally demanding, and that its success depends on the choice of reaction coordinate. By choosing a wrong Q , the system samples the wrong part of the phase space and as a consequence the rate value is not reliable.

Transition Path Sampling (TPS) [27, 28, 29] later has been developed to solve this

problem. In TPS, two states are defined by means of the order parameter and then generation of an ensemble of trajectories between initial and final states using Monte Carlo simulation in the trajectory space is performed. In this method, the order parameter does not need to be the true reaction coordinate and also we can compute the rate constant in rare events without prior knowledge of the reaction process. However, knowledge of the steady state phase space distribution is required for the acceptance or rejection step in MC. The drawback of TPS is that the calculation of the rate constant is time consuming. Although this technique needs an order parameter to distinguish two states, the order parameter has to determine whether the system is in A or B , but not where it is in between.

Moroni and co-workers developed this method further and called it Transition Interface Sampling (TIS) [30, 31, 32]. In this method, a series of interfaces (hyper-surfaces) are fixed between the initial and final states. Probability of crossing interfaces are used to estimate rate constants. These authors have also developed a method that is called Partial Path TIS (PPTIS) [33]. Using this technique, we can predict not only rate constants, but gives us free energy barriers too [34]. Moroni and coworkers used this method to study crystal nucleation of the Lennard-Jones fluid [35].

Forward Flux Sampling (FFS) [5, 7, 6] that we used in this thesis is a novel simulation technique which was developed by Allen and coworkers in order to study rare events. This method allows us to predict rate constants and follow trajectories and pathways for rare events in both equilibrium and non-equilibrium systems with stochastic dynamics. Similar to TIS and PPTIS, FFS uses a series of interfaces between initial and final states to compute the rate constant.

In the next part, we describe forward flux sampling, the technique we have used to study homogeneous and heterogeneous crystal nucleation in hard sphere colloidal suspensions. We used FFS to predict crystal nucleation rates and analyze the pathways during nucleation and growth processes.

2.3.1 Forward flux sampling

FFS technique was developed by Allen and coworkers in order to study rare events in the soft matter and the biophysical related systems. This method gives us this possibility to compute transition rates between two states and also analyze the pathways between two phases. It should be mentioned that FFS does not involve the calculation of a free energy barrier, which makes it suitable for the study of equilibrium processes. As a start point, we assume two states, the metastable phase A and stable phase B in the phase space (Fig. 2.5). Next, it is necessary to define an order parameter Q - function of the phase space coordinate - to distinguish phases A and B and define the boundary of these phases. We used the number of particles in the largest solid cluster n as the order

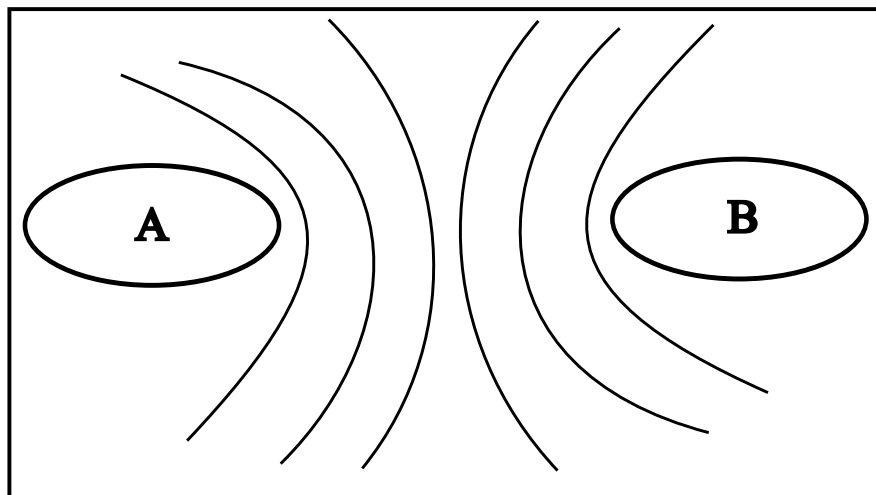


Figure 2.5: Schematic phases A and B and also interfaces between these two phases are shown. Each interface corresponds to the given cluster size n as the order parameter Q .

parameter in studies of crystal nucleation. In the next step, we divide the phase space with different interfaces with a unique number of cluster size as the order parameter. Currently we can define two stable phases by means of Q . The system is in A state whenever $Q = \lambda_A < \lambda_0$, where we define λ_0 as the boundary of state A . On the other hand, whenever $Q = \lambda_B > \lambda_n$, the system is in phase B and λ_n is defined as a boundary of phase B .

Since the transition from A to B is a rare event, when we use conventional Monte Carlo or molecular dynamics simulations, most of the time Q is smaller than λ_0 . However, the idea in FFS is to use a series of interfaces in phase space which are defined by a value of the order parameter Q ($Q = \lambda_0, \lambda_1, \dots, \lambda_n$) to drive system from A state to the state B .

The next step after identification of interfaces is to perform a brute-force simulation in meta-stable state A . When the system reaches the interface λ_0 , the configurations of the system are stored. Also we sampled the time τ which the system crosses λ_0 for the first time. The next time measurement τ is whenever the system returns to state A (i.e. coming from λ_0 and crossing λ_A) and again crossing λ_A and reaches boundary λ_0 . At the end of this part of simulations, we have a distribution of coordinates of the system in different times at the first interface λ_0 (a) part in Fig. 2.6). This distribution of configurations, is used as a random set of trajectories from the first interface λ_0 . Each trajectory is continued until the system either crosses the next interface λ_1 , or returns to the state A (b) part in Fig. 2.6). When the trajectories cross the next interface, configurations are saved again and points are called successful shots.

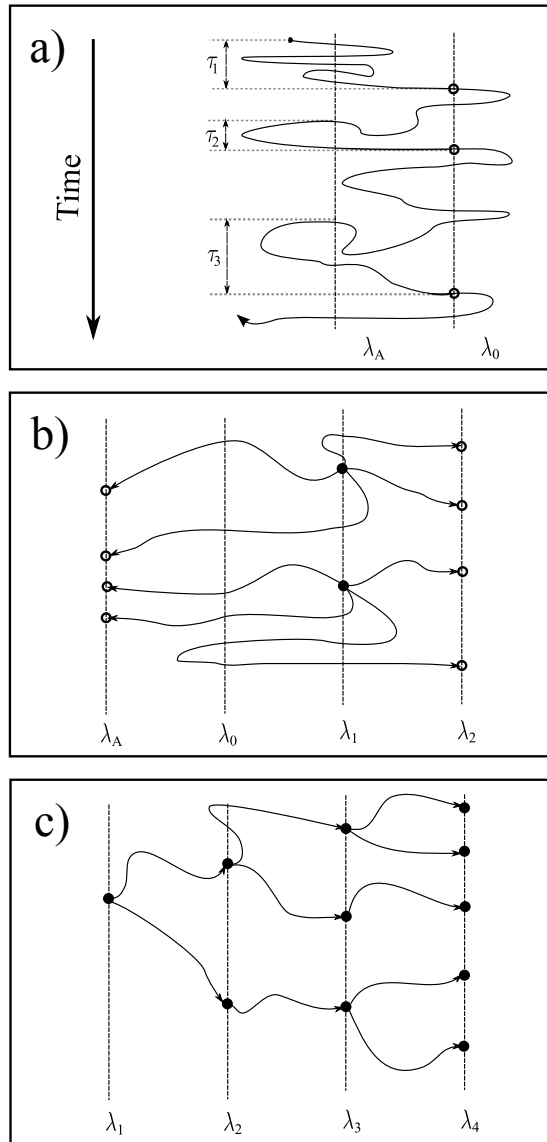


Figure 2.6: Schematic representation of the various stages during forward flux sampling. *a)* Sampling of the flux through the first interface. The crossing time τ and also stored configuration (open circles) at the first interface are sketched. *b)* Shooting of trial trajectories from saved configurations (filled circles). Some trajectories are successful and reach the next interface, but some of them are not successful and return back to the initial state (open circles). *c)* final path reconstruction connecting trajectories across interfaces.

We can continue the same procedure for all interfaces and for each interface i , compute the probability $P(\lambda_i|\lambda_{i+1})$, which is the probability of the crossing interface $i + 1$, for a trajectory that comes from state A , before it returns again to state A . Figure 2.6 (c) shows the saved configurations in different interfaces and crossing phase space to reach the final state B . In this manner all interfaces are sampled sequentially and a product of probabilities is obtained.

In FFS, the nucleation rate constants are computed as a product of two terms. One of them is the flux of stochastic trajectories which leaves the initial state A and reaches the boundary λ_0 for the first time. The next term is the probability of reaching the final state B . The rate constant R then can be written as

$$R = \Phi_{A \rightarrow 0} \cdot P_{0 \rightarrow B} = \Phi_{A \rightarrow 0} \cdot \prod_{i=0}^{n-1} P_{i \rightarrow i+1} \quad (2.35)$$

where $\Phi_{A \rightarrow 0}$ is the steady state flux of trajectories crossing the state A boundary, and $P_{0 \rightarrow B}$ is the overall probability of reaching the last interface, from trajectories which come from the initial state A .

In practice, the flux is the number of trajectories crossing boundary λ_0 per unit of time τ and volume V ($N_{A \rightarrow 0}$). In the simulation this part can be calculated from conventional MC or MD in state A :

$$\Phi_{A \rightarrow 0} = \frac{N_{A \rightarrow 0}}{t \cdot V}. \quad (2.36)$$

where $N_{A \rightarrow 0}$ is the number of saved configuration at interface λ_0 , V the volume of simulation box, and $t = \langle \tau \rangle$ is the average time the system spends in basin A before crossing λ_0 for the first time.

For calculating the probabilities, the $N_0 = N_{A \rightarrow 0}$, configurations saved at the first interface are used as start points to cross the next interface λ_1 . For each trajectory, we use M_0 independent runs with different random seed numbers from random number generator to improve statistics. The total number of trial runs are $M_0 \cdot N_0$ and we assumed the minimum number of successful runs or trajectories which reach λ_1 is $N_{0 \rightarrow 1}^{succ}$. A trajectory or run can reach the next interface or return back to the state A . The probability to reach the interface is then

$$P_{0 \rightarrow 1} = \frac{N_{0 \rightarrow 1}^{succ}}{M_0 \cdot N_0}. \quad (2.37)$$

In the next step, $N_{0 \rightarrow 1}^{succ}$ configurations are used as a starting point to estimate the probability to go from interface λ_1 to λ_2 ($P_{1 \rightarrow 2}$), and so on until the system reaches the final state B (λ_n). By calculating the flux and the overall probability, and using Eq. 2.35, we can compute rate constants. Also as we have configurations of the system

in each interface, it is possible to analyze pathways too.

2.4 Identification of crystalline clusters: Local bond order parameter

In the previous section we reviewed the forward flux sampling method for the study of rare events and particularly for the crystal nucleation phenomenon. As mentioned there, this technique requires an order parameter for identification of different states in phase space. The criteria for a good order parameter differs in different method. For some methods, such as transition path sampling (TPS) [27, 29] it is sufficient to identify start and final points of the transition in the metastable and the stable phases. On the other hand, for some other methods like forward flux sampling or umbrella sampling (US) [12] it is essential that the order parameter correlates closely with the transition progress and that it increases monotonously moving along the paths from the A state to the B .

Definition of order parameter is also essential for identification of solid-like particles and crystalline clusters. For this reason, we use a bond-order parameter analysis that was initially introduced by Steinhardt *et.al* [36] to describe the orientational order in liquids. This approach later on was extended by ten Wolde *et.al* [37] to study homogeneous crystal nucleation from a supercooled Lennard-Jones liquid. This method has the following advantages and features: first of all, it is sensitive to the difference between liquid and solid structures. Second, it does not depend on the orientation or its position in space of the crystal and is only sensitive to the overall degree of crystallinity in the system and is not sensitive to any specific crystal structure. The last important advantage is that these bond order parameters can be constructed so as to be independent from the reference frame.

In studying crystal nucleation, we use this bond-order parameter to identify the largest cluster of the new phase. We consider the size of the largest cluster to be the relevant order parameter to follows the liquid to the solid transition. In practice, we start by identifying liquid- or solid-like particles and then use a cluster definition to group neighboring solid-like particles into crystalline clusters. Finally, we chose the size of the largest cluster in the system as a local bond-order parameter (reaction coordinate Q) which follows the transition. In what follows, we will review the definition of the bond-order parameter and identification of solid clusters.

In the first step, we identify the nearest neighbors for each particle " i ". The Voronoi construction is one way to define nearest neighbors if their Wigner-Seitz cells share a face (or a line in 2D). However, this model is computationally rather expensive and time consuming. A simpler definition is based only on the particles' distance. In this case,

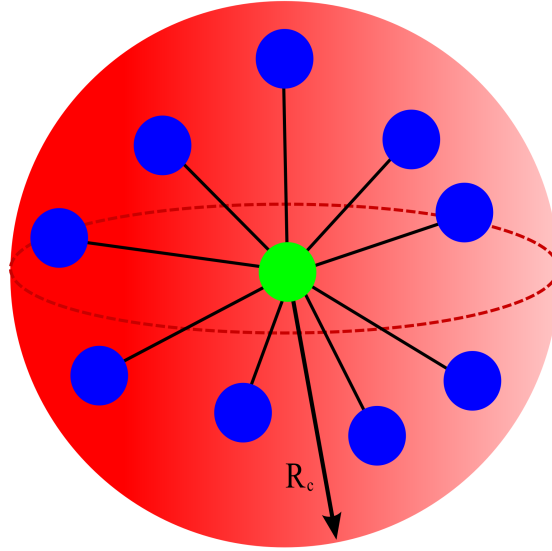


Figure 2.7: Schematic three dimensional representation of a particle surrounded by its neighbors. R_c is the radius of the sphere and used as a cut-off value for definition of neighboring particles.

we used a cut-off corresponding to the first minimum of radial distribution function $g(r)$ in the solid state at coexistence. All particles inside a sphere with radius R_c around particles i are its neighbors. Figure 2.7 shows the schematic picture of particle i and its neighbors inside the sphere with radius R_c . The local spatial orientation $\mathbf{q}_{lm}(i)$ for particle i which is a $(2l + 1)$ -dimensional complex vector, is also defined as:

$$\mathbf{q}_{lm}(i) = \frac{1}{N_b(i)} \sum_{j=1}^{N_b(i)} Y_{lm}(\hat{\mathbf{r}}_{ij}) \quad (2.38)$$

where the sum goes over all neighboring particles (named as $N_b(i)$) of particle i and $Y_{lm}(\hat{\mathbf{r}}_{ij})$ are spherical harmonics evaluated for normalized direction vector $\hat{\mathbf{r}}_{ij}$ between neighboring particles. The orientation of the unit vector $\hat{\mathbf{r}}_{ij}$ is determined by the polar and azimuthal angles θ_{ij} and ϕ_{ij} . The order l also depends on the symmetry of the lattice and must be chosen accurately. For example, *bcc* and *fcc* lattice are well respected using $l = 6$, but for the instance diamond lattice which is anti-symmetric, order $l = 3$ is better suited. Components m of the spherical harmonics also range from $-l \leq m \leq l$. The rotationally invariant local bond parameters are then defined as follows

$$q_l(i) = \left(\frac{4\pi}{2l+1} \sum_{m=-l}^{m=l} |q_{lm}(i)|^2 \right)^{1/2} \quad (2.39)$$

By this definition, we can obtain a quantity that is invariant versus both translation and

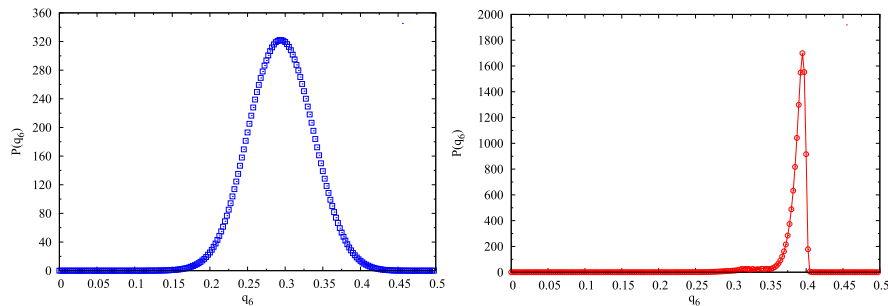


Figure 2.8: Typical distribution function of the q_6 bond order parameter from MC simulations in a hard sphere system. Here we used $R_c = 1.4\sigma$ for the local environment of each particle. The right-hand side is for a system in the solid state ($\beta P\sigma^3 = 20.00$) and the left side illustration is for a system in the liquid state ($\beta P\sigma^3 = 10.00$)

rotation and does not depend on the frame of reference. This is an important property, since a crystal cluster can form anywhere in the system and with any orientation. In Fig. 2.8 we show typical distribution function of the local bond-order parameter from Monte Carlo simulation of a hard sphere system close to the coexistence. The figure shows that there is some separation between probability distribution function in solid and liquid states, however, there is some overlap too and separation is never pronounced. We can enhance this separation of the distribution function by calculating the correlation function of the vector \mathbf{q}_6 of the neighboring particles i and j

$$\mathbf{q}_6(i) \cdot \mathbf{q}_6(j) = \sum_{m=-6}^{m=6} q_{6m}(i) \cdot q_{6m}(j)^* \quad (2.40)$$

where the $*$ is the complex conjugate. Figure 2.9 shows the corresponding distribution function of $\mathbf{q}_6(i) \cdot \mathbf{q}_6(j)$ for the hard sphere system. Although the distributions are distinct, ten Wolde *et.al* [38] suggest additional criterion for identification solid-like particles. They have mentioned if $\mathbf{q}_6(i) \cdot \mathbf{q}_6(j)$ for particles i and j is larger than a particular threshold (In our case, for hard sphere this number is around 0.7 as shown in Fig. 2.9), these two particles are connected. We count the number of connections between particles (n_b) and define solid-like particle as a particle with at least $n_b = 6$ (Fig. 2.10).

In the last step we need to have a criterion to define clusters in the system. The usual criterion is that if particles i and j are solid-like particles and are less distant than a cut off value R_c , then they are in the same solid cluster. The procedure is repeated over all solid-like particles. Finally we use the number of particles in largest the cluster (n^*) as the order parameter (reaction coordinate) in forward flux sampling to describe the transition from meta-stable liquid phase to crystalline state.

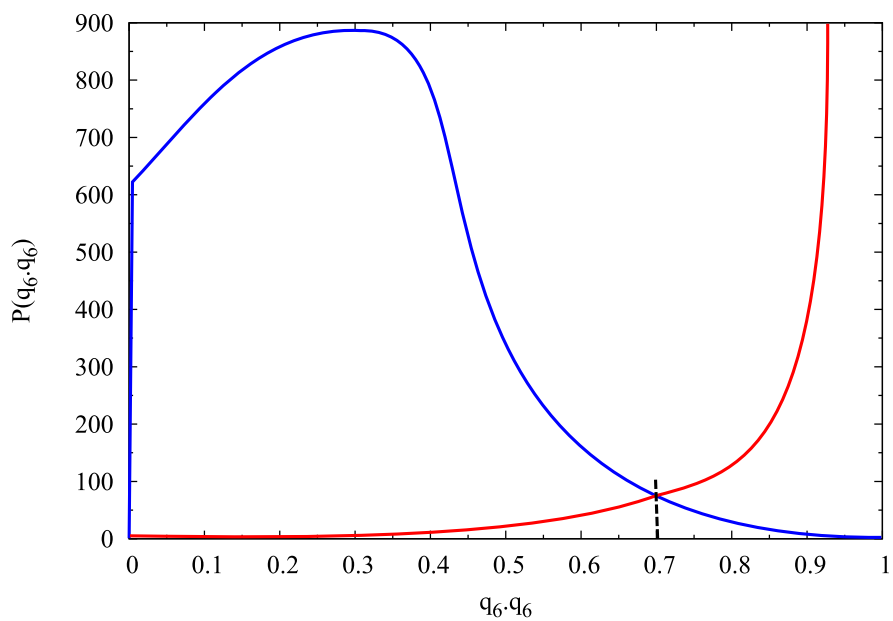


Figure 2.9: Probability distribution function (PDF) of $\mathbf{q}_6(i) \cdot \mathbf{q}_6(j)$ for hard sphere system from MC simulation results

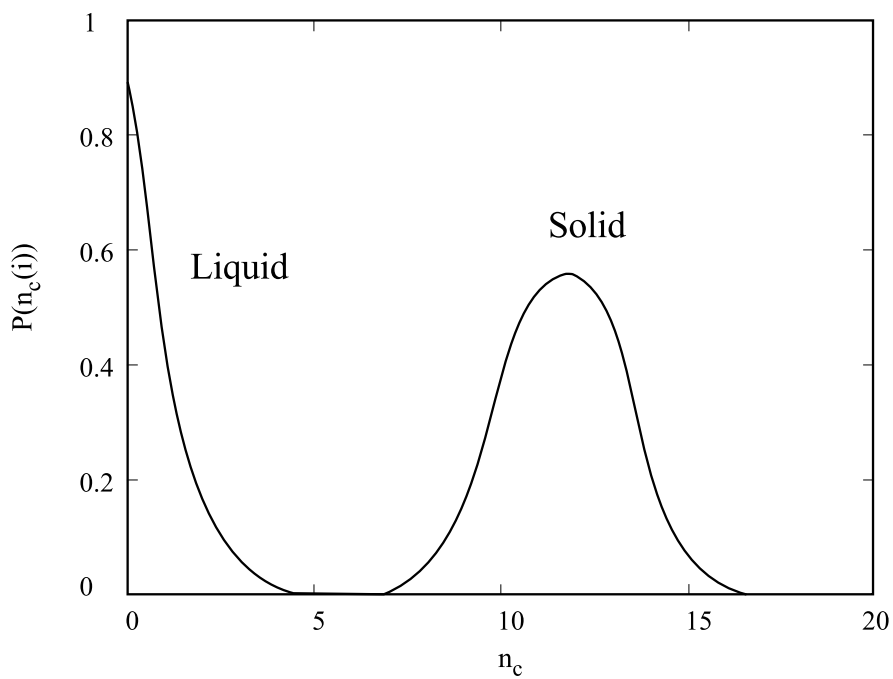


Figure 2.10: Probability distribution of the number of connections per particle for a meta-stable liquid and solid state.

3 Determination of crystal nucleation rates of hard sphere suspensions

Using computer simulation, we study the homogeneous crystal nucleation of supersaturated hard sphere colloidal suspensions. The crystal nucleation rates are determined by Monte Carlo simulations using the forward flux sampling (FFS) technique. We compare computed rate constants with experimental data and other theoretical results. Results are presented for the effect of the degree of supersaturation on the nucleation rates and critical cluster sizes. We also compare the obtained value for critical Gibbs-free energy barrier with classical nucleation theory and umbrella sampling. At the end of this chapter we analyze the crystalline cluster by computing gyration tensor.

3.1 Introduction

Nucleation [39] as a transformation in first order phase transition, is an interesting phenomenon and it was studied extensively during last decades. This phenomenon occurs when a system which is in the meta-stable state, by a rare fluctuation (fluctuation in density, pressure, etc.) passes a barrier in energy of the system and transforms to the stable state. Nucleation phenomenon in the nature, is classified into two major categories. In one case, the nucleation is observing in the bulk and because of fluctuations in the system that is called "homogeneous" nucleation. The second one which is more common in the nature is "heterogeneous" nucleation. In heterogeneous nucleation, because of contacting system with external objects or forces, either something in solution or dust in the air or walls of the container, the system nucleate and the phase transition in the system is occur.

Nucleation in colloidal systems, is an example of this phase transformation. There are several colloidal models that have been studied to explain nucleation from theoretical and experimental point of view. As a simple model, hard sphere model has a crucial role in condensed matter physics and material sciences, since it successfully gives the essential and fundamental structural properties of fluids, crystals, glasses, colloidal suspensions and granular media. Experimentally the phase behaviour of hard sphere suspensions has been examined by Pusey and van Meegen [40]. They found the freezing volume fraction of hard sphere is $\eta = 0.495$ and the melting volume fraction of hard sphere suspensions is $\eta = 0.545$. These values are in agreement with the theoretical prediction of Hoover and Ree for fluid-solid transition of hard spheres [41].

Also from theoretical point of view, hard sphere suspensions are interesting to study. The main reason of interest is the application of hard spheres in predicting many natural behavior of simple fluids and soft matters [42]. Note that hard sphere systems are simple models in colloidal physics and they are reference systems for studying the behavior of more complicated fluids. Thermodynamic properties of hard sphere systems have been investigated in the past decade. The coexistence pressure [43, 44, 45, 46], kinetics growth coefficients [47], interracial free energies [48, 49, 50, 51], crystallization of hard spheres, for both homogeneous [13, 52, 53, 54] and heterogeneous [55, 56, 57] cases studied using computer simulations.

The nucleation rate for hard sphere systems, is one of the interesting quantities to investigate and study. This quantity has been measured experimentally, using different methods like light scattering [16, 17, 18]. Also Confocal microscopy is used to give a direct access to particles positions, similar as in simulation and therefore any quantity of interest can be obtained from the trajectory and position of particles [58, 59, 60, 61]. Polymethylmethacrylate (PMMA) as a hard sphere particles in a liquid mixture of decaline and carbon disulfide is the usual system for studying hard spheres in lab [16,

58].

On the other hand, nucleation rates are predicted theoretically by using computer simulations. Auer and Frenkel [13] have used umbrella sampling (US) technique to study homogeneous nucleation in hard sphere systems, in order to determine homogeneous crystal nucleation rates in moderate under-cooling. Also, Schilling *et al.* and Filion *et al.* used brute-force Monte Carlo and molecular dynamics to predict nucleation rates of hard sphere suspensions in high supersaturations [15, 14].

In this chapter, we present the study of homogeneous crystal nucleation in moderate degrees of supersaturation to predict crystal nucleation rates and analyze growing crystal clusters by using forward flux sampling [5, 6, 7]. In practice and for simulations, we used the same conditions as Auer and Frenkel used in their work [13].

The chapter is arranged as follows. In Sec. 3.2 we outline simulation method and computational details. We then present in Sec. 3.3 result of FFS for prediction of crystal nucleation rates and analysis of crystalline clusters. Section 3.4 summarizes our conclusions.

3.2 Computational methodology and simulation strategies

The system that we shall consider in this work is the suspension of spheres interacting via the hard sphere potential. For a colloidal system of mono-disperse hard spheres with diameter σ , the hard core interaction potential is defined as

$$u(r) = \begin{cases} \infty & r < \sigma \\ 0 & r \geq \sigma \end{cases} \quad (3.1)$$

where r is a distance between two center of mass of particles. Since any configuration of the hard sphere system has zero potential energy, the fluid-solid transition in such system is completely driven by the entropy and temperature T only plays the role of the energy scale. Hence, density (ρ) or packing fraction $\eta = (\pi\sigma^3/6)(N/V)$ is the only quantity for controlling the thermodynamic properties of such system (or we can use the pressure P in the NPT ensemble for which the total volume V fluctuate).

Our simulations operate within the isothermal-isobaric (N, P, T) ensemble, wherein the particle number N , pressure P and the temperature T are constant while the system volume V fluctuates. For the system, we used a cubic box with 13824 hard core particles inside it and periodic boundary conditions in all directions. MC simulations were carried out using the standard Metropolis algorithm to equilibrate the system [62, 63]. Similar to the work of Ref. [13] and for comparison, we study crystal nucleation for three different pressures $\beta P\sigma^3 = 15.00$, $\beta P\sigma^3 = 16.00$ and $\beta P\sigma^3 = 17.00$ corresponding to different supersaturations ($\Delta\mu = 0.34$, 0.44 and 0.54). In MC moves, the trial move

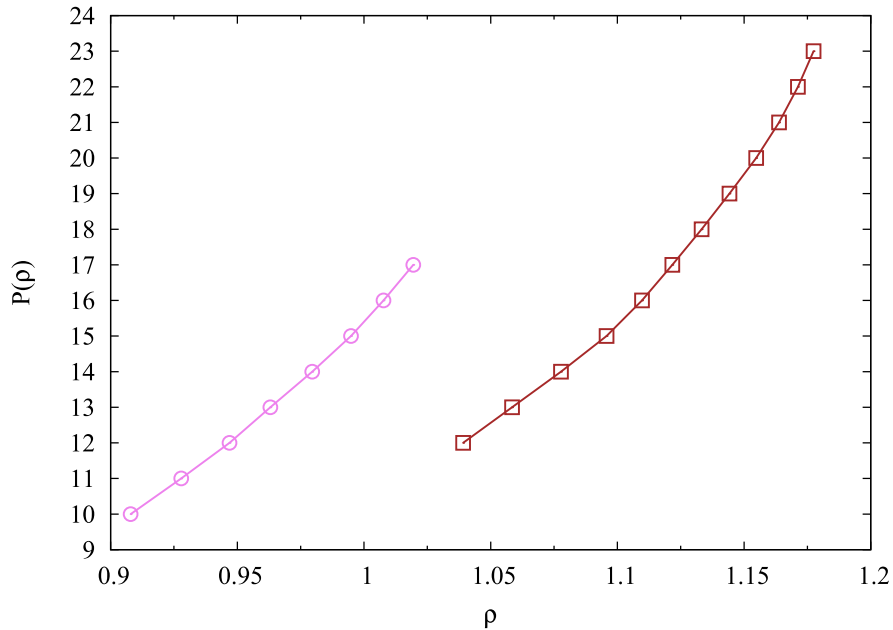


Figure 3.1: Equation of state of bulk hard sphere system at constant pressure and constant temperature.

size was chosen to be $\Delta x = 0.05\sigma$ and volume move was chosen $\Delta V = 0.00005\sigma^3$. Also we used 1×10^{-6} sweeps for equilibration, and sampled observables every 2000 sweeps. The results for the fluid and the crystal phases are presented in Fig. 3.1.

Since nucleation in the moderate super-cooling is a rare event, it is difficult to study with brute-force Monte Carlo or molecular dynamics at low supersaturations (Fig. 3.2). Hence we applied forward flux sampling technique with Monte Carlo simulation to study crystal nucleation from the super-cooled liquid.

In the simulation of fluid-solid transition, in order to distinguish between colloidal particles in the liquid and the solid phases, we used q_6q_6 -bond-orientational order parameter (local bond-order parameter) [36, 37] which is one of the well characterized order-parameter to identify the solid-like and the liquid-like local order around a colloidal particles. This identification has been applied to study nucleation [37, 64, 54]. In nucleation, the number of solid-like particles in the largest cluster is used as a reaction coordinate Q .

Then we apply the forward flux sampling method, a rare event technique developed by Allen *et al.* [5, 6, 7] to determine crystal nucleation rates and configuration pathways in the phase space. In our simulations, to have accurate statistics, all calculation for nucleation rates and estimation of critical cluster sizes are averaged over ten independent FFS simulation runs. Also in each run, at least 60 successful pass per interface are used. Here the errors in cluster sizes are given by the FFS interface spacing. The size of

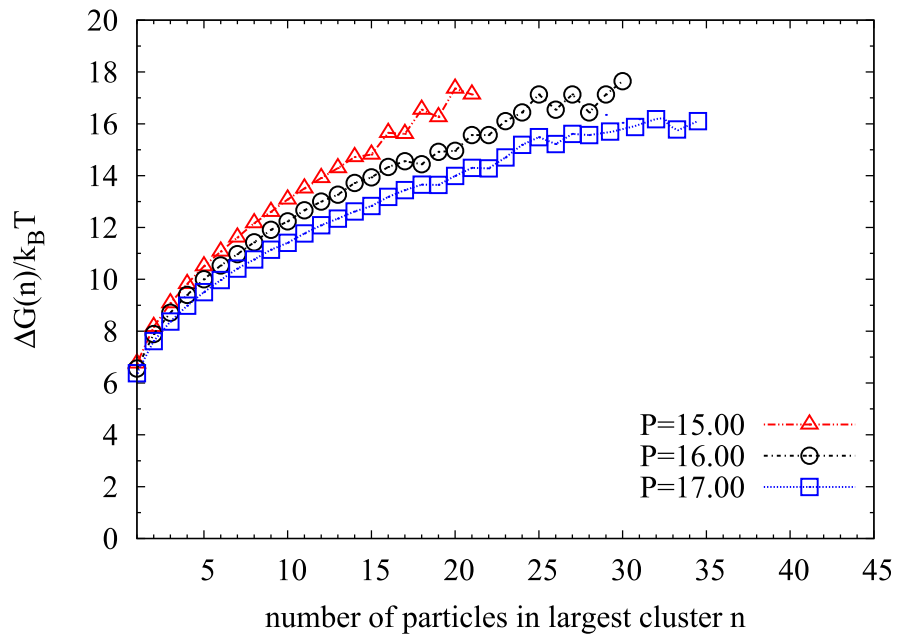


Figure 3.2: Measurements of the Gibbs free-energy $\Delta G(n)/k_B T$ as a function cluster size n from brute-force Monte Carlo simulations in a system of hard sphere at three different pressures. As shown, there are some small clusters observed in the system at different pressures. Computed values for n and also Gibbs free-energies are lower than the CNT predictions.

the critical nucleus is also computed by corresponding value of the reaction coordinate of the FFS interface at which the probability to reach the final state exceeds 0.5 [65].

Figure 3.3 shows a snapshot of the hard sphere system including solid clusters inside. The snapshot is for a system at the pressure $\beta P\sigma^3 = 16.00$ with a critical cluster in it. Note that the size of all particles in the Fig. 3.3 is the same and to observe clusters inside the system, we showed liquid particles in the system by black points. Also solid-like particles with high ($n_b > 10$) and low ($6 \leq N_b \leq 10$) symmetry are shown with different sizes and colors.

3.3 Results and discussion

In this section, we describe our results from forward flux sampling simulations of crystal nucleation of hard spheres in moderate supersaturations. Monte Carlo simulation method in the isobaric-isothermal ensemble (NPT) is performed to determine the crystal nucleation rates and to trace the trajectory of pathways in the phase space. Since the bulk coexistence pressure for the hard sphere is about $\beta P_{coex}\sigma^3 = 11.67$ [41], the corresponding degrees of supersaturation that we used, are $\Delta P = P - P_{coex} = 3.33$, 4.33 and 5.33. FFS technique is a way to overcome Gibbs free-energy barriers and computing nucleation rates.

In the first step, we used well-equilibrated configurations of the system in the liquid metastable state. $n = \lambda_0$ is chosen from brute-force simulation results (as shown in Fig. 3.2 small clusters are existed in the system). Then we implemented brute force Monte Carlo simulations and we collected $N_0 = 60$ configurations at the first interface (λ_0) to measure the flux. Also in order to compute the flux, the total time consumed by the system in the liquid basin, neglecting the time spent at the boundary λ_0 . In the final step, the stored configurations (N_0) at the first interface are used as start points to compute the probability of reaching the final state. We assumed at least $M_0 = 60$ stochastic trajectories are crossing each interface (Table 3.1).

Table 3.1: Computational details used in FFS simulation runs.

Pressure $\beta P\sigma^3$	Number of interfaces	λ_0	N_0	M_0
15.00	60	10	60	60
16.00	48	12	60	60
17.00	34	15	60	60

According to the forward flux sampling, the rate constant can be written as

$$R = \Phi_{A \rightarrow 0} \cdot P_{0 \rightarrow B} = \Phi_{A \rightarrow 0} \cdot \prod_{i=0}^{n-1} P_{i \rightarrow i+1}, \quad (3.2)$$

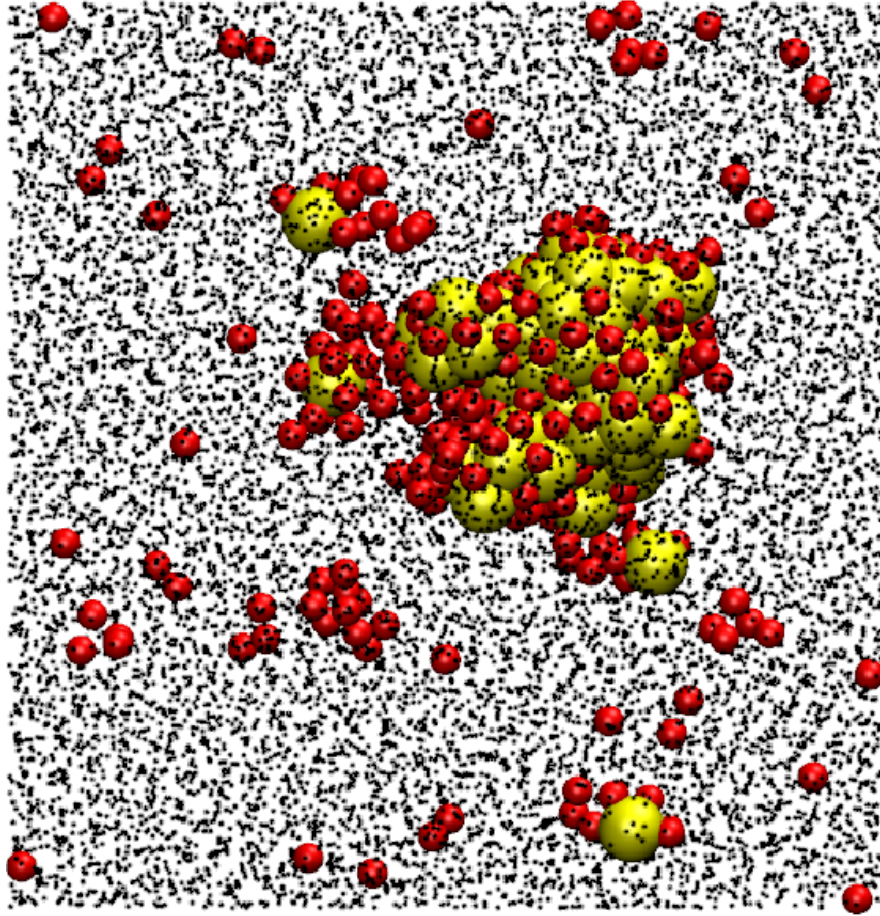


Figure 3.3: Snapshot of a hard sphere system with $N = 13824$ colloidal suspensions containing a critical cluster size at a liquid pressure $\beta P \sigma^3 = 16.00$. Perfect solid-like particles ($n_b > 10$) are shown in yellow. Solid-like particles with low symmetry ($6 \leq N_b \leq 10$) are shown in red and for liquid-like particles we used black points. Note that the size of all particles are the same and different range has no physical meaning.

where $\Phi_{A \rightarrow 0}$ is steady state flux of trajectories crossing the state A boundary in the unit of volume and the unit of time, and $P_{0 \rightarrow B}$ is the overall probability of reaching the last interface, from trajectories which come from the initial liquid state. Figure 3.4 shows FFS results of the probability of reaching the cluster size n ($P(n)$) as a function of the number of particles in the largest cluster n . Each point is averaged over at least ten independent FFS simulation runs. As is shown in Fig. 3.4, at the beginning of the process, crystallization of clusters is difficult and clusters like to shrink and return to the liquid state. Therefore the probability of reaching next interfaces is low. However, after reaching the critical cluster size, the probability of crossing interfaces is high (almost near one) and clusters like to grow and reach the next interfaces. Finally, by using Eq. 3.2, we can compute the crystal nucleation rates for hard spheres in given degrees of supersaturation (Table 3.2).

Figure 3.5 shows the density of different configurations in different interfaces for a system in $\beta P \sigma^3 = 17.00$. As is shown, different trajectories of configurations exist in the phase space. At the beginning of the process, when largest clusters are small, configurations are more correlated and in principle, all new configurations are created from the same parent configurations and, they have the same thermodynamical properties like the bulk density. For configurations with large clusters (bigger than the critical cluster) in the growth process, the story is different. Here different systems choose different ways and therefore many branches of trajectories in the phase space occur.

The size of critical nuclei is another quantity that we can obtain from FFS results. The critical nucleus size in the forward flux sampling is approximated as an interface nearest to where the probability of reaching final state for the largest clusters exceeds 0.5. Therefore stored configurations in such interface have critical cluster sizes. Averaging over all largest clusters in such interface ($M_0 = 60$ configurations), we can predict the average critical cluster size (n^*) in such systems. Errors in critical cluster sizes are equal to the distance between interfaces. FFS results for different pressures in the moderate supersaturation are listed in Table 3.2.

Table 3.2: Summary of FFS simulation results of homogeneous crystal nucleation for the hard sphere system in different degrees of supersaturation.

Pressure $\beta P \sigma^3$	critical cluster size n^*	Zeldovich factor Z	$\Delta G_{FFS}^*/k_B T$	Nucleation rate $k \sigma^3 \tau_L$
15.00	218 ± 10	9.1×10^{-3}	36.02	1.23×10^{-17}
16.00	126 ± 5	1.4×10^{-2}	24.89	1.10×10^{-12}
17.00	109 ± 5	1.6×10^{-2}	15.73	1.18×10^{-8}

In the next part, we compare FFS results of crystal nucleation rates with other theoretical predictions and experimental data. Figure 3.6 shows the comparison of our

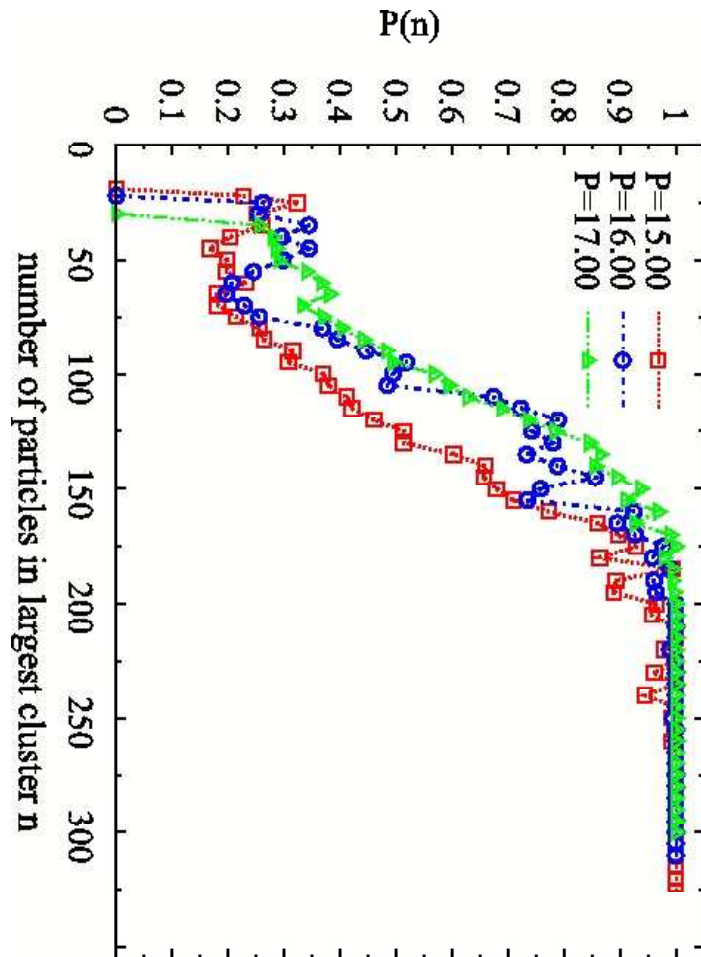


Figure 3.4: FFS results of the probability of reaching cluster size n as a function of number of particles in the largest cluster n for different systems in pressures $\beta P\sigma^3 = 15.00$, 16.00 and 17.00 .

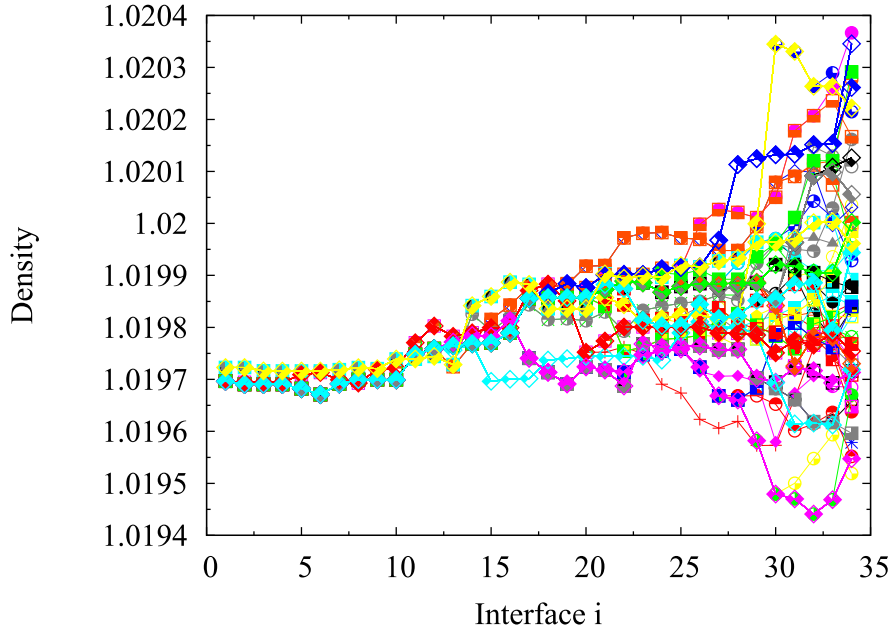


Figure 3.5: Density of different systems in different pathways in the phase space. The x axis shows the interface id in phase space and y axis is the density of systems. Results are for one FFS run for a system with $\beta P \sigma^3 = 17.00$.

results with experimental results of Harland and van Megen [16], Sinn *et al.* [17] and Schätzel and Ackerson [18] and also umbrella sampling simulations of monodisperse and 5% polydisperse hard sphere suspensions studied by Auer and Frenkel [13] and brute force MC and MD [14, 15] for high supersaturations. We used the scaled value of the experimental volume fractions and also the polydisperse results of Auer and Frenkel to yield coexistence densities of monodisperse hard spheres [66, 67, 14]. In Fig. 3.6, we plotted nucleation rates in the unit of the long time diffusion coefficient ($\tau_L = \sigma^2/6D_L$) as a function of the volume fraction (η). To compute diffusion coefficients, we calculated mean square displacement (MSD) for the system in different pressures and then we extracted the diffusion coefficient by using the Einstein equation (Fig. 3.7). Einstein equation in three dimensions can be written as

$$D_L = \frac{1}{6} \lim_{t \rightarrow \infty} \frac{d}{dt}(MSD). \quad (3.3)$$

Note that error bars in Fig. 3.6 are not shown in this plot. For FFS results, the error is between 2 and 4 orders of magnitude. As is shown in Fig. 3.6, FFS simulation results are in agreement with results of umbrella sampling, however there is a significant difference between FFS results and experimental data in low supersaturations. It should mention that the origin of this discrepancy between theoretical results and experimental data for low degrees of supersaturation is not clear yet.

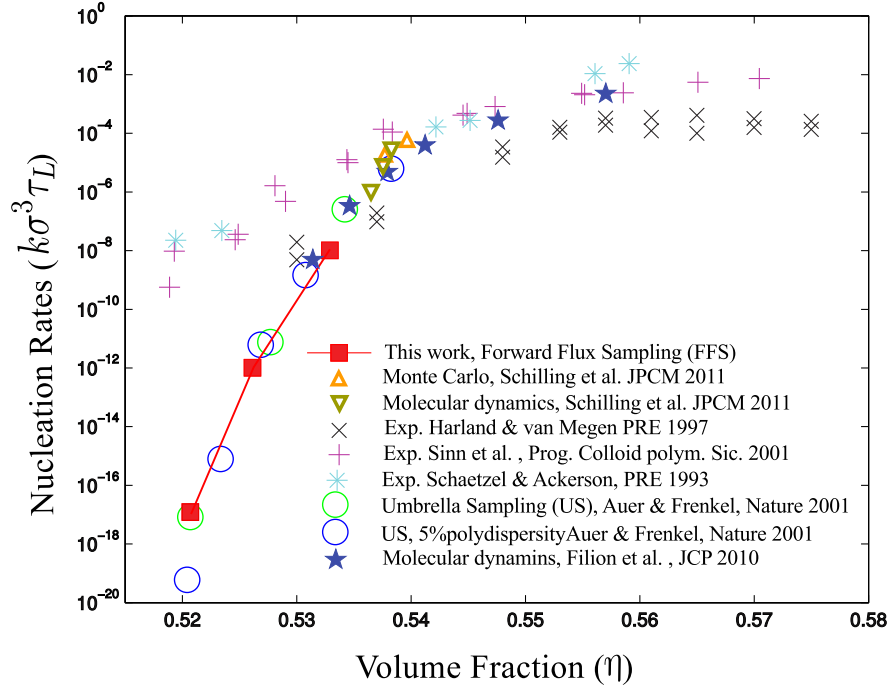


Figure 3.6: FFS results of crystal nucleation rates for hard sphere systems compare to the experimental results from Refs. [16, 17, 18] and theoretical data from US simulation of Ref. [13] and brute force MC and MD [14, 15].

As explained in previous chapter, in the classical nucleation theory, the maximum value for the Gibbs free energy barrier is defined as

$$\Delta G^* = \frac{16\pi}{3} \frac{\gamma_{ls}^3}{(|\Delta\mu|\rho_s)^2}. \quad (3.4)$$

where $|\Delta\mu|$ is difference in the chemical potential between the liquid state and the solid state from Table 3.2. The height of free energy barrier in the FFS can be approximated from the CNT expression for rate as follows [65]

$$\Delta G_{FFS}^* = -k_B T \ln(k_{FFS}/J_0), \quad (3.5)$$

where J_0 is the kinetic pre factor which can be approximated by [68]

$$J_0 \approx Z\rho_l^2 DR^*. \quad (3.6)$$

In Eq. 3.6, D is the self diffusion coefficient and Z is the Zeldovich factor [24] and can be defined as:

$$Z = \left(\frac{|\Delta G''(n)|_{n^*}}{2\pi k_B T} \right)^{1/2} = \left(\frac{|\Delta\mu|}{6\pi k_B T n^*} \right)^{1/2}. \quad (3.7)$$

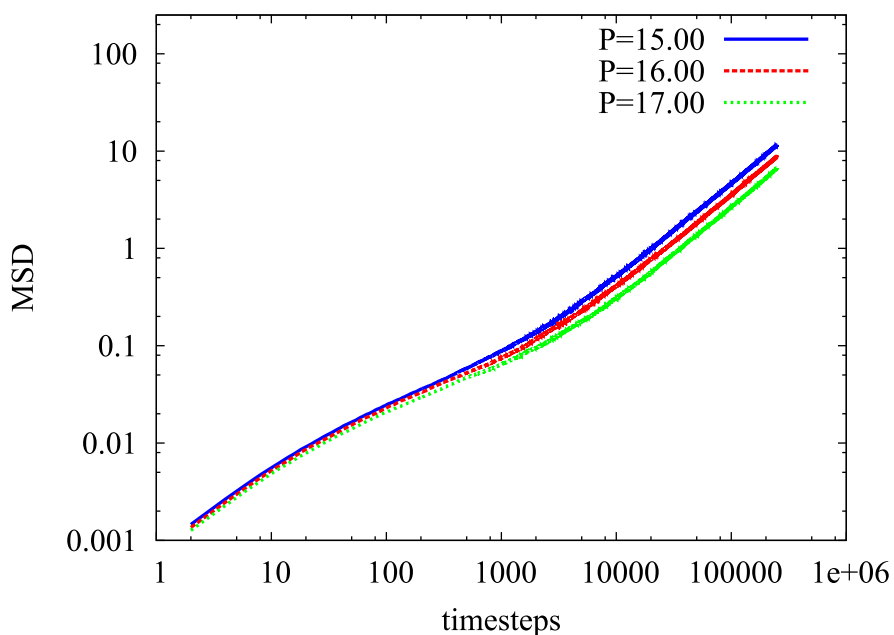


Figure 3.7: Mean square displacement (MSD) as a function of time steps are shown for three different pressures. MSD is defined as $MSD = \langle r^2(t) \rangle = \langle \frac{1}{N} \sum_{i=1}^N (r_i(t) - r_i(0))^2 \rangle$. Here, N is the number of particles, t corresponds to time, and $r_i(t) - r_i(0)$ is the vector distance traveled by a given particle over the time interval. The slope of the MSD, considered for long time intervals, is related to the self-diffusion constant D_L (Eq. 3.3).

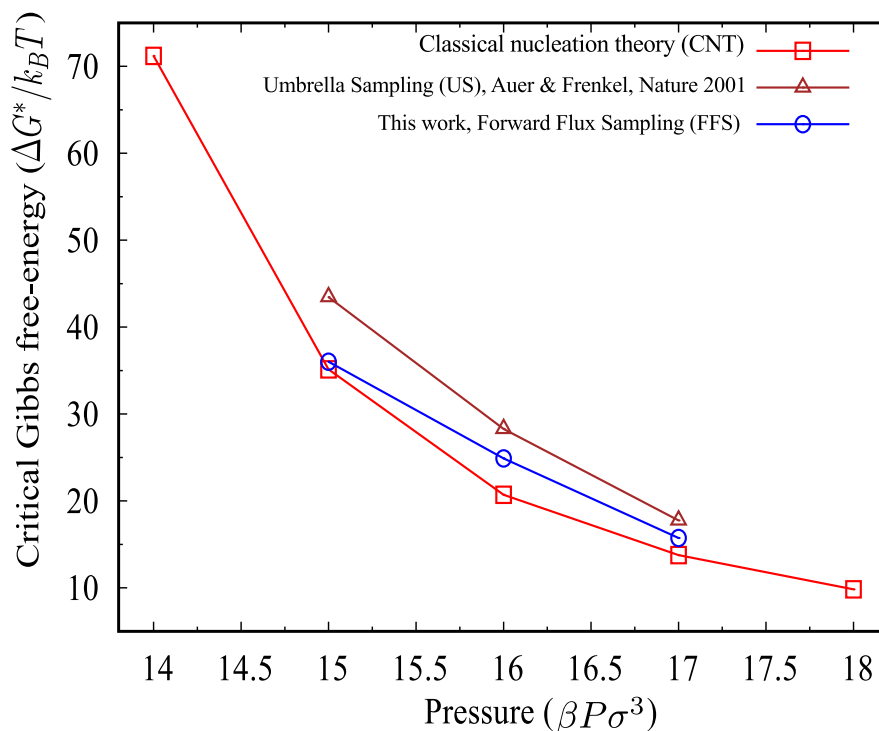


Figure 3.8: The height of Gibbs free energy barrier is plotted as a function of pressure. Comparison of CNT predictions with the US simulation and FFS results are shown.

We used Eq. 3.5 and data from Table 3.2, to compute Zeldovich factor and critical Gibbs free energy barriers from FFS results (Table 3.2) and then compare our results with the classical nucleation theory and umbrella sampling data [52]. Figure 3.8 shows the height of Gibbs free barrier as a function of the pressure. Classical nucleation theory, umbrella sampling and FFS results for critical Gibbs free energies are shown and as we can see, there are acceptable agreements between FFS results with US and CNT predictions. CNT assumptions can be a reason for small difference between FFS results and CNT predictions.

In the last part of this chapter, crystalline clusters in the system are analyzed. As in the FFS we save all configurations in the nucleation process, we can analyze shape and form of clusters in the system. At the start point, since we are interested in the shape of critical nuclei, we focus on different configurations of hard sphere systems that have the critical largest cluster. FFS results show that critical clusters have different shapes. As we know from classical nucleation theory assumptions, clusters in such systems are spherical, however, analysis of clusters shows that in reality, critical clusters with the same sizes have different forms and they are not completely spherical. Figure 3.9 shows a typical snapshot of critical clusters for three different pressures. Note that

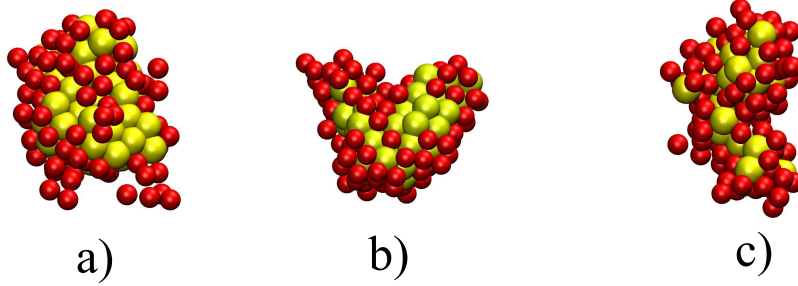


Figure 3.9: Typical Snapshots of critical nucleus for a system in (a) $\beta P\sigma^3 = 15.00$, (b) $\beta P\sigma^3 = 16.00$ and (c) is for $\beta P\sigma^3 = 17.00$. Yellow particles have more than 10 solid-like neighbors ($n_b > 10$) and red ones have $5 < n_b < 10$ solid-like particles as a neighbor.

liquid particles around the cluster are not shown. Particles with more than 10 solid-like neighbors ($n_b > 10$) are shown by the yellow colour. These particles are almost in middle of clusters. Red particles have $5 < n_b < 10$ solid-like particles as a neighbor and they are more on the surface of clusters.

The evaluation of the shape of growing crystalline cluster can be studied quantitatively by computing the gyration tensor, \hat{X} for the largest cluster and for different interfaces in the phase space. Tensor of gyration is defined as the root mean square distance of the particle in the cluster from its center of mass. \hat{X} can be written as

$$X_{\alpha,\beta} = \frac{1}{N} \sum_{i=1}^N S_i^\alpha S_i^\beta, \quad \mathbf{S}_i = \mathbf{r}_i - \mathbf{R}_{c.m}, \quad \alpha, \beta = x, y, z. \quad (3.8)$$

where \mathbf{r}_i labels the coordinate of effective particle i belonging to the cluster with N solid particles in it and $\mathbf{R}_{c.m}$ is the position of the central mass of the cluster. We calculated elements of the gyration tensor for all configurations in pathways and then we averaged over all configurations in the same interface (with the same number of particles in the largest cluster). We found that, clusters have different shapes and forms. Also small clusters are more elongated and larger ones are more compact and have an ellipsoidal shape rather than the spherical form. The radius of gyration of the cluster given by $R_g^2 = Tr\hat{X} = \langle X_{xx} \rangle + \langle X_{yy} \rangle + \langle X_{zz} \rangle$, is shown in Fig. 3.10 as a function of the cluster size n over all sampled configurations. In data for all pressures there is spread in radius of gyration. At the beginning of transformation and for small clusters, there is a wide spread, but, for big clusters, the spread in the radius of gyration decreases. Figure 3.11 shows the mean value of the radius of gyration as a function of the cluster size n . Again we averaged over all configurations in the same interface. By increasing the size of largest cluster in the system, the radius of gyration increases. $\langle R_g \rangle$ at the beginning of process, for small cluster sizes increases faster and then

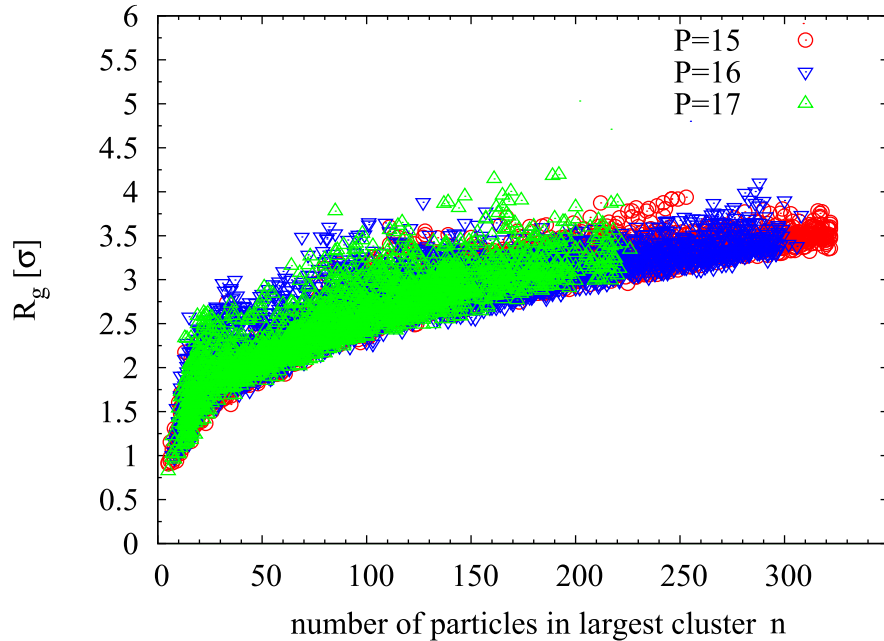


Figure 3.10: Radius of gyration of the largest crystal cluster R_g versus number of particles in largest cluster n for the hard sphere system in three different pressures $\beta P \sigma^3 = 15, 16, 17$.

follows the fix rate of increasing.

3.4 Conclusion

In this chapter, we presented an accurate approach to determine crystal nucleation rates of super-cooled hard sphere colloidal suspensions by using the forward flux sampling (FFS) technique for different degrees of supersaturation. Even at the same degree of under-cooling, we found a good agreement between the rate constant we obtained with the FFS comparing to umbrella sampling (US) results in Ref. [13]. We also compared FFS results for crystal nucleation rates with conventional molecular dynamic and Monte Carlo simulations and also with experimental data. Similar to results of the umbrella sampling, for low supersaturations, the discrepancy between numerical results and experimental data exists and the origin of this discrepancy is unclear yet. But it can be argued that the discrepancy is not because of the numerical method and computational difficulties. Also a comparison of critical Gibbs free energy barriers for hard sphere systems between FFS results, with US data and classical nucleation theory predictions was done. FFS results are near and a bit higher than the CNT predictions. The CNT assumptions can be the reason for this small difference.

On the other hand, analysis of the biggest clusters in the system by means of gyration

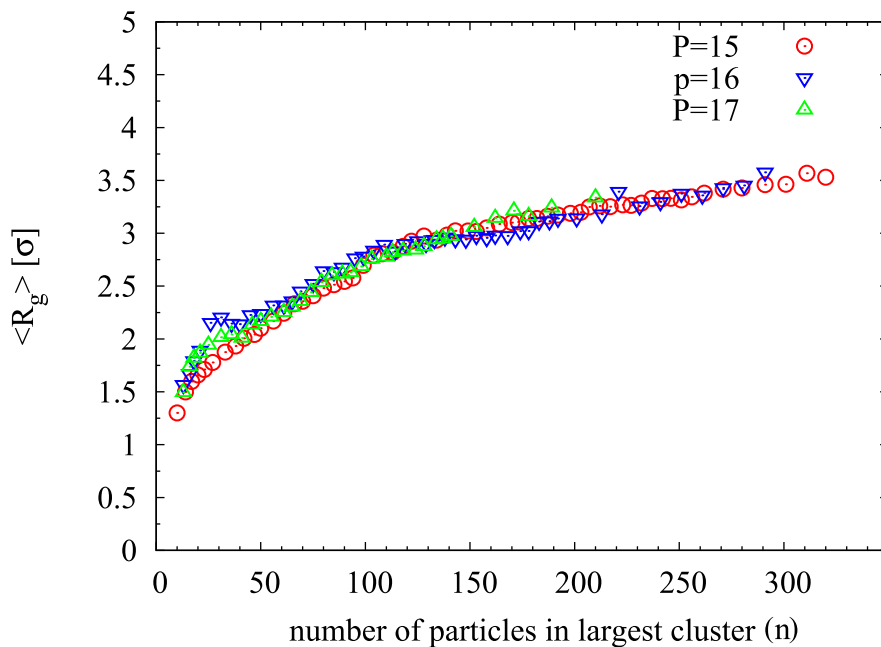


Figure 3.11: Average radius of gyration $\langle R_g \rangle$ as a function of largest cluster size (n) for the hard sphere system in pressures $\beta P \sigma^3 = 15, 16, 17$.

tensor was made. These analysis indicate that for the small size of nuclei, clusters are more elongated in one arbitrary direction. However, by increasing number of particles, clusters become more compact and with ellipsoidal form.

4 Heterogeneous nucleation of hard sphere system at the hard wall

In this chapter we use computer simulation in order to study heterogeneous crystal nucleation. Monte Carlo simulation study of a hard sphere colloidal system confined in a pore formed by one bcc (100) structured wall and one uniform repulsive plane is discussed. Constant-temperature, constant-normal-pressure ($NP_{\perp}T$) ensemble is performed to study heterogeneous crystal nucleation in such system. We compute crystal nucleation rates for the hard sphere system in moderate supersaturations using forward flux sampling (FFS) technique. We also analyze solid clusters in the system by calculating components of gyration tensor and predict a rough estimation of contact angles in different degrees of supersaturation. Also for all systems, the averaged contact angles are high and as a consequence, crystallization of hard spheres in such system are happening via heterogeneous nucleation.

4.1 Introduction

In practice many first order transitions, such as condensation and crystallization, occur via heterogeneous nucleation [69, 70]. The nucleus of the new phase forms in contact with the wall of container, impurity or any other external effect. In principle, heterogeneous nucleation at walls or impurities needs to be separated from homogeneous nucleation in the bulk, and small changes in parameters leads to large change in nucleation rates. In the case of heterogeneous nucleation at the wall, the structure and properties of the wall control the rate of nucleation.

The Vollmer's classical theory of nucleation in the case of heterogeneous nucleation was extended by Turnbull, Fisher [2, 71]. They used CNT to study the heterogeneous nucleation at the wall. Later on, Fletcher [72] used this theory to deal with nucleation on spherical impurities of arbitrary size.

Same as homogeneous nucleation, the hard sphere model is used to study heterogeneous nucleation. Such systems as mentioned in previous chapter, has been studied in great detail and its bulk properties is well understood. However, the behavior of such system in confinement and near hard wall is less clear. The behaviour of fluids in contact with substrates plays an important role in areas of wetting, adhesion, and heterogeneous nucleation [73, 74]. For the heterogeneous nucleation, more work was focused on exploring the influence of planar structureless wall on crystal nucleation and surface freezing [56, 73]. Also in some work crystallization of hard sphere system at patterned substrates was studied [75, 76, 77]. Effects of different wall structures on crystallization of hard sphere colloidal particles were the main focus points on these researches. However, studying of heterogeneous nucleation to determine nucleation rates and examine the effect of the wall on structural properties of crystalline clusters have not been well characterized.

In this context, we study the heterogeneous nucleation of the hard sphere colloidal system, near the structured bcc(100) wall using forward-flux-sampling (FFS) technique [5, 6, 7]. We applied the FFS technique to predict heterogeneous nucleation rates for different degrees of supersaturation. FFS yields nucleation rates rather than free energy barriers and allows to estimate the size of the critical nucleus directly from simulation data. Here we predicted the rate of nucleation for different degrees of metastability, and we analyzed crystalline clusters. Also a rough estimation for the contact angle of crystalline clusters at the structured bcc wall was done.

The outline of this chapter is as follows: in Sec. II we describe the simulation model and computational details. In section III we present FFS results for heterogeneous nucleation rates and also we discuss the analyzed properties of clusters, while Section IV presents and summarizes our conclusions.

4.2 Computational methodology and details

In order to study heterogeneous nucleation, we used the Monte Carlo method for a system of hard sphere colloidal particles confined in a pore with wall separation L_z . The wall area is fixed at $L_x L_y = 1506.48$. L_z is fluctuating, but it is much larger than any correlation length in the fluid. Then, we performed MC simulations in $(NP_{\perp}T)$ ensemble where the temperature, number of particles and the pressure perpendicular to the wall were kept constant and the volume was allowed to fluctuate in z direction. The system consists of $N = 12672$ mono-dispersed particles confined between a structured bcc (100) wall and a structureless wall. The interaction between particles is hard core. As we are interested to study heterogeneous nucleation at the structured wall, to avoid the effect of the planar wall and finite size effects, we used a repulsive interaction between particles and the flat wall. The interaction is defined as follows

$$u_w(r) = a[\tanh(\frac{z - z_0}{w}) + 1] \quad (4.1)$$

where $a = 20$ and $w = 2.0$ are constant and z_0 is the position of the flat wall. The interaction between the wall and particles are cut at cutoff distance $r_c = 5.0\sigma$. Applying the repulsive interaction, decreases the effect of the planar wall in the nucleation process at the wall. Figure 4.1 shows the density profile of a hard sphere confined between one bcc structured wall and one repulsive planar wall in the liquid state ($\beta P\sigma^3 = 11.00$). As is shown, because of the repulsive interaction, there is no liquid layer at the planar wall and as a consequence the effect of this wall on particles in the system is disappeared.

For the structured wall, an impurity of N_w hard sphere particles in the bcc (100) structure was placed into the system as a hard wall with the lattice spacing $a = 1.5\sigma$. we used the z axis in the direction perpendicular to the plane of impurities and the flat wall. The interaction between fixed particles and other colloidal particles in the system is also hard core. Figure 4.2 shows a schematic snapshot of the system.

Similar to the case of the homogeneous nucleation, in the first step we computed the equation of state for such system by using brute-force MC. Then we chose three different pressures $\beta P\sigma^3 = 12.00, 12.50$ and 13.00 , corresponding to different supersaturations. Periodic boundary conditions applied to x and y directions of the simulation box. Other computational conditions are the same as we did in the homogeneous case.

Next, the FFS method [5, 6, 7] was used to capture heterogeneous nucleation pathways and estimate heterogeneous crystal nucleation rates. Critical cluster sizes are also computed by the value of reaction coordinate of the FFS interface at which the probability to reach the final state exceeds 0.5 [65]. Here we used the number of solid-like particles in the largest cluster as a reaction coordinate Q . Furthermore, to identify solid- and fluid-like particles and then colloidal clusters, we applied local-bond orien-

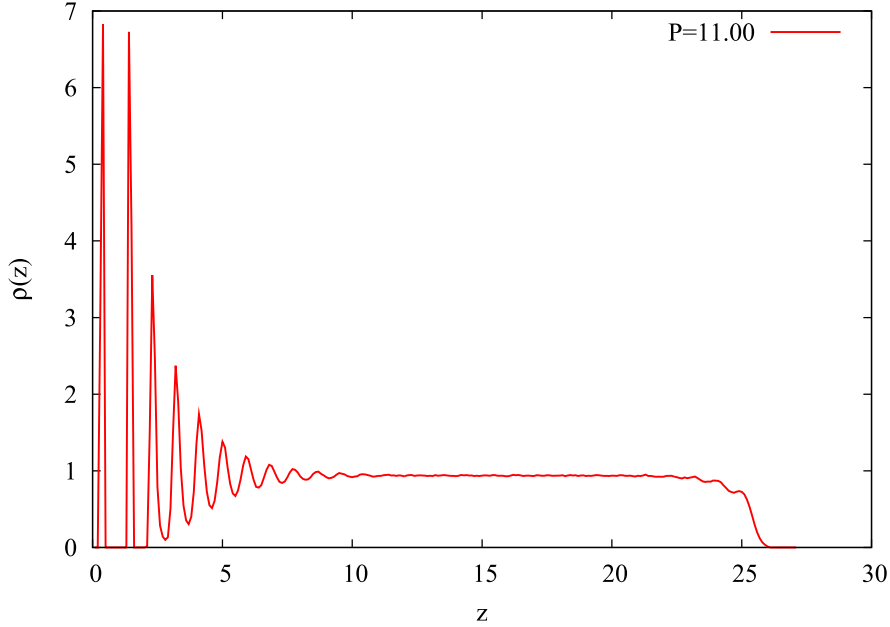


Figure 4.1: Density profile $\rho(z)$ of the liquid phase of hard spheres in confinement at $P = 11.00$. Repulsive planar wall, decreases the effect of wall on crystallization and heterogeneous nucleation process. Two first peaks corresponds to the wall layers.

tational order parameter [36, 37]. All calculations for nucleation rates and estimation of critical cluster sizes are averaged over ten independent FFS simulation runs with at least 50 successful pass per interface.

4.3 Results and discussion

In this chapter, we investigate heterogeneous crystal nucleation at the structured hard wall. Monte Carlo simulation in the isobaric-isothermal ensemble ($NP_{\perp}T$) is used to compute crystal nucleation rates at three different pressures $\beta P \sigma^3 = 12.00$, 12.50, and 13.00. Since the bulk coexistence pressure for hard spheres is $\beta P_{coex} \sigma^3 = 11.67$ [41], corresponding degrees of supersaturation are $\Delta P = P - P_{coex} = 0.33$, 0.83 and 1.33. For these pressures, due to existence of free energy barriers, nucleation process is not accessible in brute force simulations. Using the FFS technique is a way to overcome such barriers and compute nucleation rates.

4.3.1 2D analysis

Existence of a wall in the system has an important role in the heterogeneous nucleation. Interaction between particles and the wall, also structure of the wall and arrangements

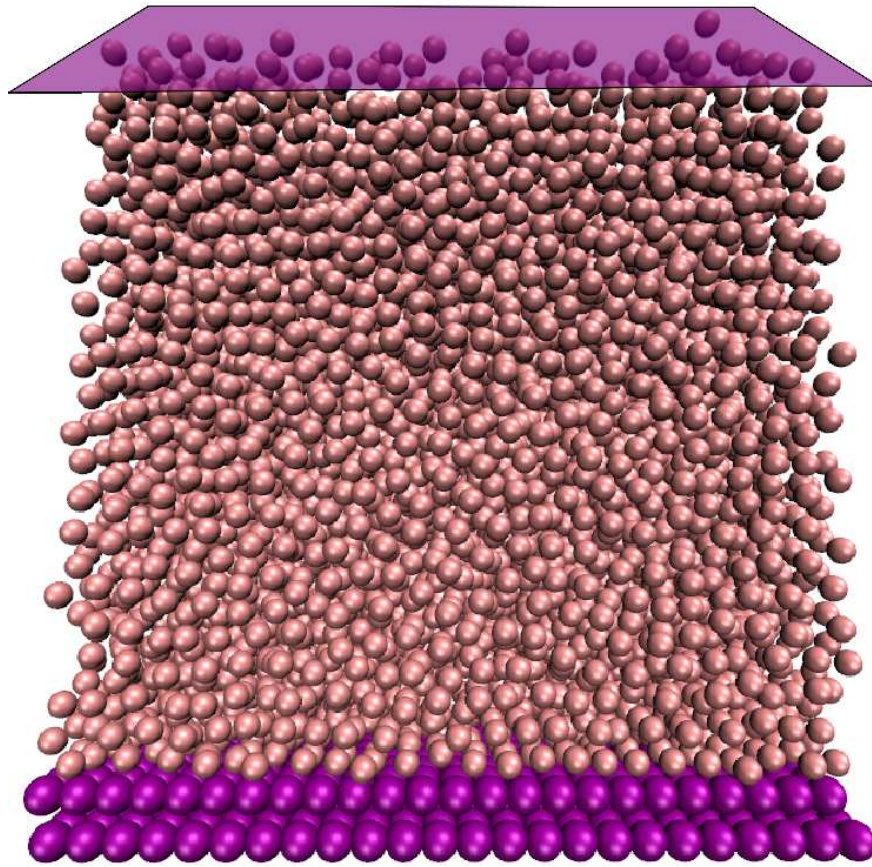


Figure 4.2: Characteristic snapshot of hard sphere colloidal system confined between one structured bcc (100) wall and one structureless wall. This picture is for a system at pressure $\beta P \sigma^3 = 11.00$.

of the particles on it can change the surface tension energy between the wall and particles in the liquid and solid states. Hence as a consequence, the crystallization process in such systems is changed. We started to study crystallization of hard sphere suspensions at different structured walls. To analyze the layering and the arrangement of particles inside the layer, we consider the bond-orientational order in two dimensions [78]: we define the local bond-orientational order parameter of particle j in layer m at a position \mathbf{x}_j as

$$\psi_6^m(\mathbf{x}_j) = \frac{1}{N_j} \sum_{k=1}^{N_j} e^{i6\theta_{jk}} , \quad (4.2)$$

where N_j is the number of neighbors of particle j within layer m , the sum is over the neighbors k of j within m , and θ_{jk} is the angle between an arbitrary fixed axis and the line connecting particles j and k . The order of the m -th layer Ψ_6^m is defined as the average over $\psi_6^m(\mathbf{x}_j)$ for all N_m particles within the layer

$$\Psi_6^m = \frac{1}{N_m} \left| \sum_{j=1}^{N_m} \psi_6^m(\mathbf{x}_j) \right| . \quad (4.3)$$

Figure 4.3 shows an example result of Ψ_6^m for the hard sphere liquid in four different pressures. These pressures are chosen to be below and also above of the coexistence bulk pressure for two different systems. One is for a system with the bcc (100) structured wall and the other is for the fcc (111) structured wall. As we see, when approaching the transition, the bond-orientational order close to the wall increases. It clearly “jumps” is discontinuous at the transition for the system with bcc (100) wall. However, for the fcc (111) system and for the pressure below the coexistence pressure, pre-solidification in the system occurs and the system is starting to become to the solid phase via layering and the system wets the structured wall. We did the same analysis for other structures and orientations (results are not shown) and came to the conclusion that bcc (100) is an advisable structure for the wall to study heterogeneous crystal nucleation.

In order to determine nucleation rates by the FFS, we applied brute force simulations in the liquid metastable state. These simulations give us configurations with at least $n = \lambda_0$ particles in the largest cluster. To increase the accuracy of simulations, $N_0 = 50$ configurations at the first interface (λ_0) are collected to measure the flux. Also we measured the total time spent by the system in the liquid basin neglecting the time spent at the boundary λ_0 . Computational details of our simulation are listed in Table 4.1.

The probability of crossing interfaces in phase space is plotted in Fig. 4.4. Points are averaged over ten independent FFS runs with at least $M_0 = 50$ successful crossing path per interface. According to Fig. 4.4, same as homogeneous nucleations, at the beginning of the process, reaching interfaces are difficult and clusters like to shrink

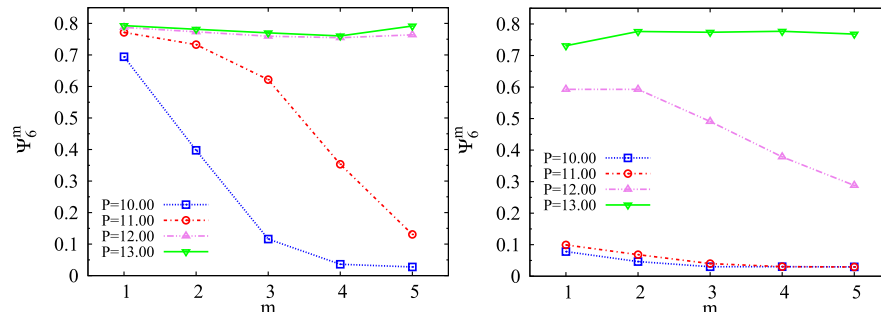


Figure 4.3: 2D bond orientation order parameter Ψ_6^m for the stable and the metastable hard sphere fluid versus the number of layer m from the structured wall for fcc (111) (the left-hand side) and bcc (100) (the right-hand side) structures.

Table 4.1: Computational details of FFS, used in simulations

$Pressure(\beta P\sigma^3)$	Number of interfaces	λ_0	N_0	M_0
12.00	65	15	50	50
12.50	65	20	50	50
13.00	50	25	50	50

and return to the liquid state. However, after crossing the critical interface and in the growth region, the probability of crossing interfaces is almost one or near it.

Table 4.2 shows results of heterogeneous crystal nucleation rates using (Eq. 2.35) and critical cluster sizes for different degrees of supersaturation.

Table 4.2: Summary of the FFS simulation results the prediction of heterogeneous crystal nucleation rates and critical nuclei in different pressures.

Pressure $\beta P\sigma^3$	Nucleation rate $k\sigma^3\tau_L$	critical cluster size n^*
12.00	9.34×10^{-14}	415 ± 10
12.50	1.18×10^{-9}	152 ± 5
13.00	4.73×10^{-8}	131 ± 5

The critical cluster size is another quantity that we can compute using the FFS method in MC simulations. In other simulation techniques, like umbrella sampling (US), the approach for achieving the critical cluster size is to calculate the free energy barrier of the system, and then predict critical cluster sizes. Unlike to US, the size of critical nucleus in FFS, is approximated to be in stored configurations in the interface nearest to where the probability to grow to the final phase exceeds 0.5. Figure 4.5 shows a typical snapshot of critical clusters for systems in three different pressures. Snapshots depicted from a view perpendicular to the bcc wall side. Violet particles in

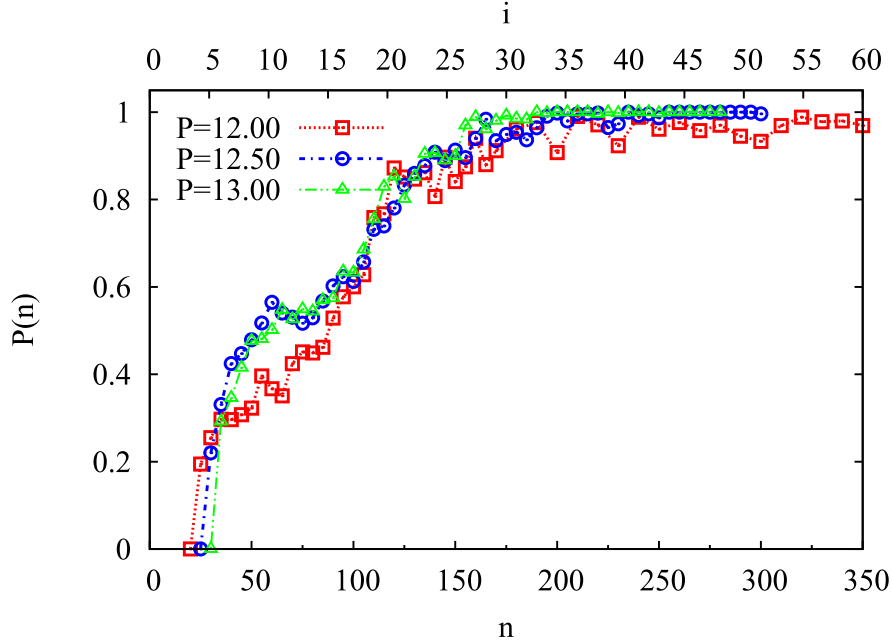


Figure 4.4: FFS results about probability of reaching cluster size n as a function of the cluster size n in different degrees of supersaturations. Results are plotted after averaging over ten runs with at least $M_0 = 50$ successful path-configurations per interface.

clusters have more than 10 solid-like neighbors ($n_b > 10$) and almost have the perfect crystal structure. Green particles have $5 < n_b < 10$ solid-like particles as neighbors. As we see, middle of clusters containing compact crystalline particles.

In the next step, we examined the saved configurations with different critical cluster inside them. Figure 4.6 shows a typical example of the computed pathway for heterogeneous nucleation at the structured bcc (100) wall. Results are for a system with $\beta P \sigma^3 = 13.00$. Largest crystalline clusters on the wall are shown from two different point of view; parallel and perpendicular to the wall. Also three different points in the phase space are chosen. Pre-critical, critical and post-critical crystal nucleus are shown. Blue particles have more than 10 solid-like neighbors ($n_b > 10$) and green particles have $5 < n_b < 10$ solid-like particles as a neighbor.

In the literature two ways for nucleation process are discussed [38, 79, 64]. The first is the growth of a single nucleus in the system and the second is via the creation of many small clusters in the systems. In our simulation results, we didn't observe the second scenario of phase transition and nucleation of a compact crystal nucleus, indicated that the first way is favored. We used also these configurations and insert some brute force Monte Carlo simulations. We observed that in many cases, the system continued the solidification process and after some time we have completed solid phase in the system,

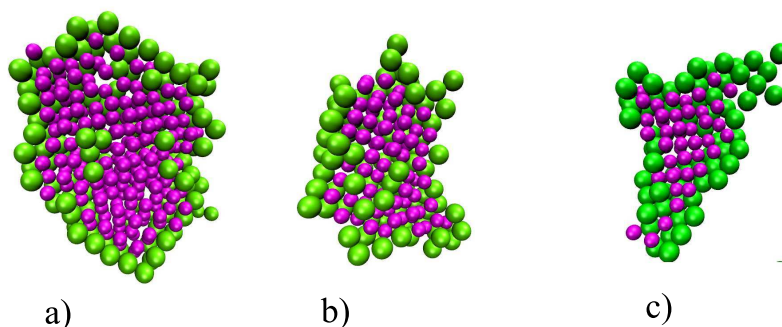


Figure 4.5: Snapshots of critical clusters at three different pressures. (a) is for $\beta P\sigma^3 = 12.00$, (b) for $\beta P\sigma^3 = 12.50$ and (c) is for $\beta P\sigma^3 = 13.00$. Pictures depicted from the view perpendicular to the bcc wall. Violet particles have more than 10 solid-like neighbors ($n_b > 10$) and green particles have $5 < n_b < 10$ solid-like particles as a neighbor

however, in some cases especially for the pressure $\beta P\sigma^3 = 12.00$, the critical cluster in the system during MC simulation runs shrinks and the system return back to the metastable liquid state.

To study the shape of clusters in the system at the structured wall in the nucleation process, we implement analysis of largest clusters by identification of the gyration tensor \hat{X} as defined in the previous chapter (Eq. 3.8). For this purpose, we computed all component of \hat{X} in three dimensions for all biggest clusters in all interfaces. Tensor of gyration describes the overall spread of the particles in solid cluster and is identified as the root mean square distance of the collection of particles from their common centre of mass. As is well-known, radius of gyration is defined as $R_g^2 = Tr\hat{X} = \langle X_{xx} \rangle + \langle X_{yy} \rangle + \langle X_{zz} \rangle$ over all sampled configurations. X_{xx} , X_{yy} and X_{zz} are computed from Eq. 3.8. Figure 4.7 shows the radius of gyration $\langle R_g^2 \rangle$ versus the number of particles in the largest cluster n in the system. Results are for different degrees of supersaturations. As is shown in Fig. 4.7, by increasing the size of largest cluster in the system, radius of gyration increases.

Comparing the behavior of radius of gyration between the bulk system and the system confined between walls is also interesting. As is shown in Figs 4.7 and 3.10, the behavior of R_g is independent of the degrees of supersaturation. Therefore we can compare bulk results and data of confined systems. The average of radius of gyration between two systems are shown in Fig. 4.8. For small cluster sizes, there is no significant difference in R_g . However for larger clusters, radius of gyration of the cluster at the wall as a function of the cluster size n , has a higher slop.

Finally, we applied gyration tensor analysis to predict a rough estimation for the contact angle between crystalline clusters and the bcc (100) structured wall. Crystalline

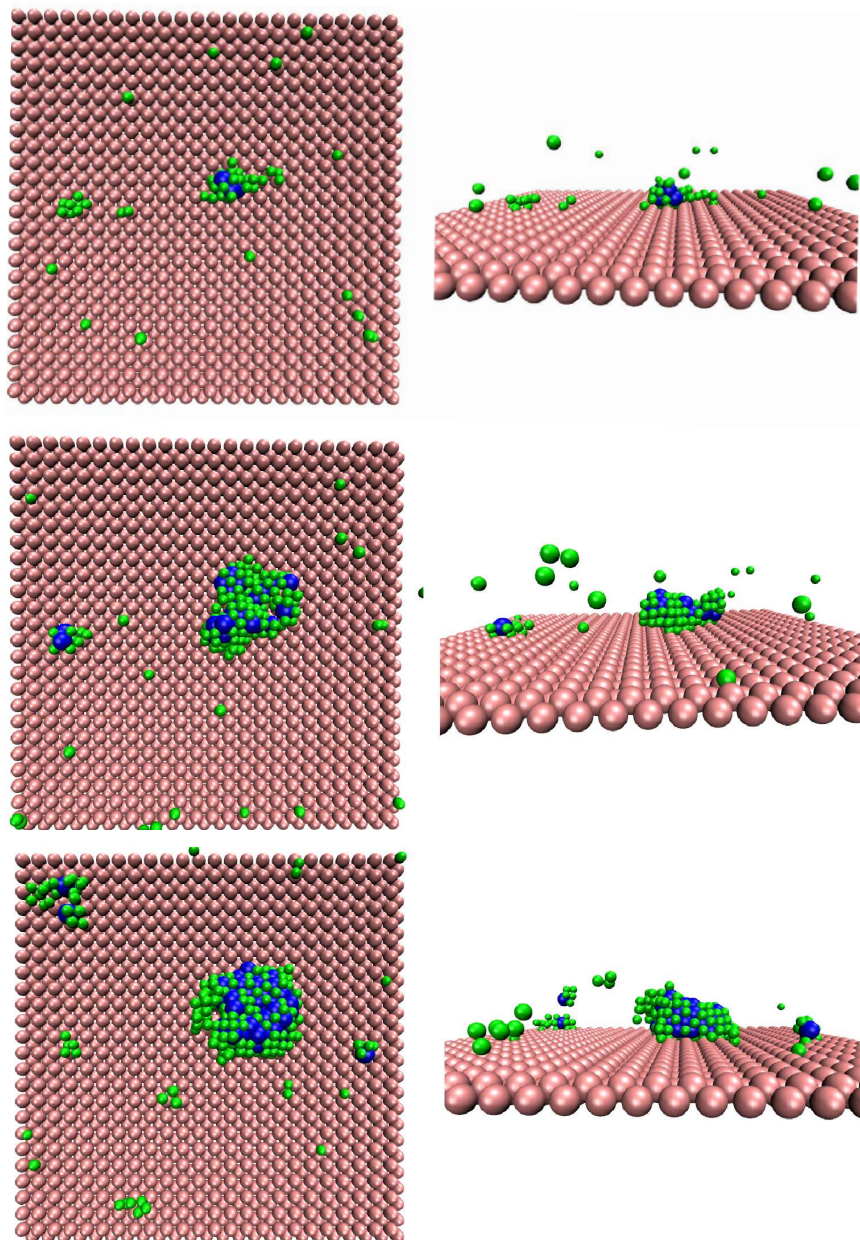


Figure 4.6: A typical snapshot of heterogeneous nucleation process of hard sphere particles at bcc(100) structured wall for a system at $\beta P\sigma^3 = 13.00$. Pictures are depicted from two different point of view, parallel and perpendicular to the wall and for three different interfaces corresponding to pre-critical, critical and post-critical nucleus. Only solid-like particles are shown. Blue particles have more than 10 solid-like neighbors ($n_b > 10$) and green particles have $5 < n_b < 10$ solid-like particles as a neighbor.

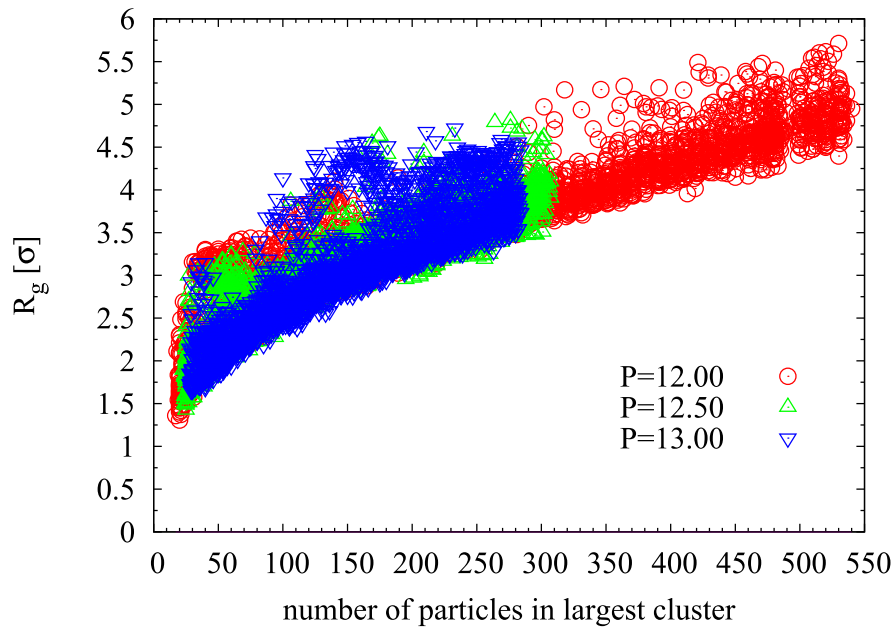


Figure 4.7: Radius of gyration for all clusters in all range of sizes as a function of the cluster size n in three different pressures $\beta P\sigma^3$.

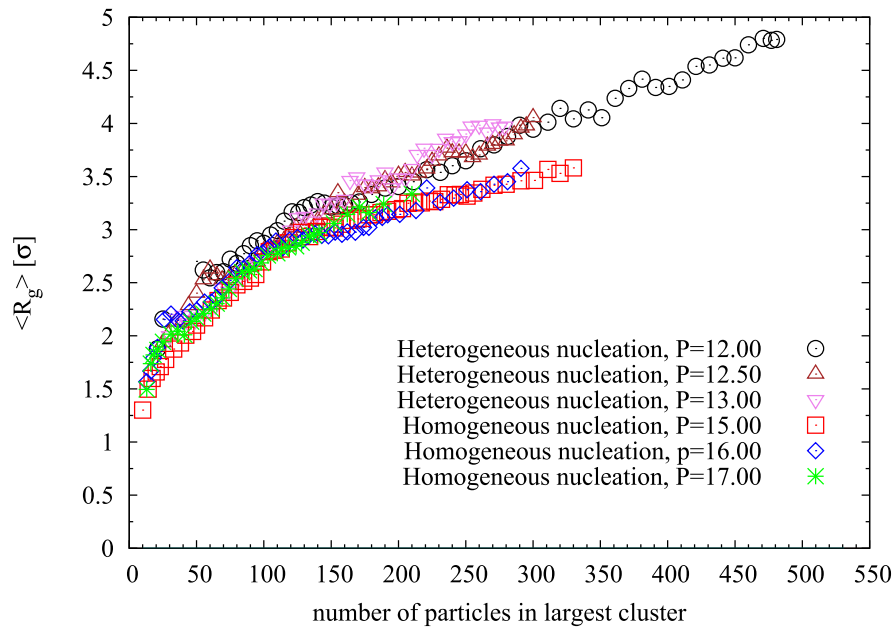


Figure 4.8: A comparison of the average of radius of gyration between homogeneous and heterogeneous crystal nuclei as a function of cluster size n in different degrees of super-cooling. We averaged over all configurations with the same number of particles in the biggest cluster.

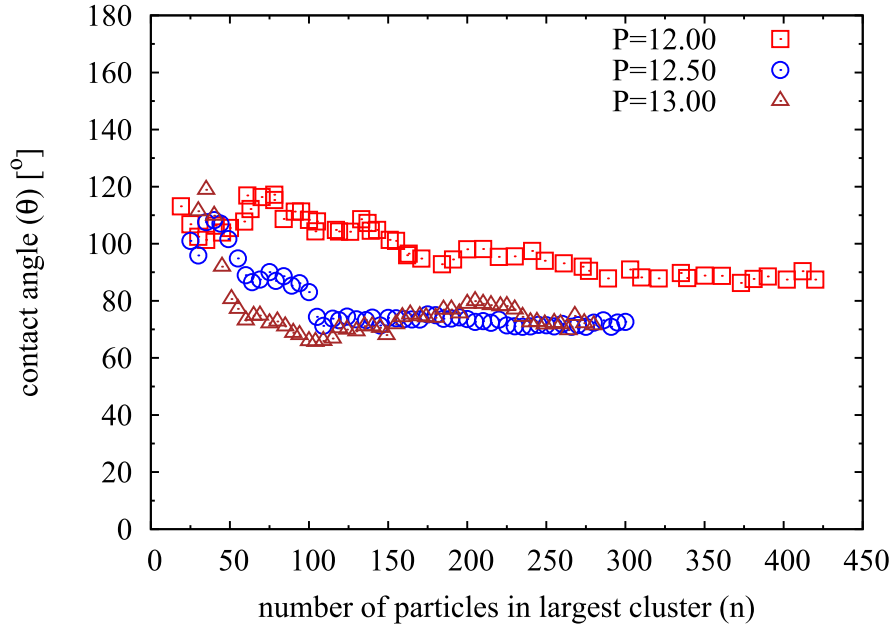


Figure 4.9: Contact angle θ [°] plotted as a function of cluster size n for different degrees of supersaturation. For each interface, all data are averaged overall at least 50 configurations

clusters at the wall have different shapes and analysis of clusters shows that for each individual interface, clusters with the same size have different forms. However, growing process of clusters depends on the thermodynamics of the system like pressure, surface tension and so on. Therefore we can estimate the contact angle of clusters in the system. Relation between contact angle and gyration tensor can be written as [80]

$$\cos(\theta) = \frac{XY - 6ZZ}{XY + 2ZZ}, \quad (4.4)$$

where XY and ZZ are two components of gyration tensor in xy plane and z direction. Figure 4.9 shows results of the contact angle between crystal clusters and the wall (θ [°]) as a function of the cluster size n . We plotted in Fig. 4.9 averaged value of contact angle over all configurations in the same interface. For small clusters, fluctuations in the contact angle is observed, however, for larger cluster sizes, these fluctuations are decreased and the contact angle shifts to the fix number. Observed contact angles show that for all three different pressures we are far from wetting region and crystallization of the hard sphere system at bcc (100) structured wall in happens via heterogeneous nucleation.

4.4 Conclusion

In this chapter, we studied the heterogeneous crystal nucleation of the hard sphere system by combining the Monte Carlo simulation technique with the forward flux sampling. In our simulations we used the number of particles in the largest crystal cluster as a reaction coordinate Q and we applied the $q_6 - q_6$ local bond order parameter to identify liquid- and solid-like particles. In the first step, we estimated the heterogeneous crystal nucleation rates for the moderate supercooled liquid. These predictions are first results for heterogeneous crystal nucleation rates in such systems. Analysis of the trajectories and saved configurations also indicate that nucleation takes place via the creation, formation and growth of a compact nucleus. These clusters have different compact shapes, however, by growing the critical clusters, they were mostly compact and had hemisphere shapes.

To determine a rough estimation of the contact angle, we analyzed the crystalline clusters by computing the gyration tensor. For different supersaturations, we found high value of contact angles. These results show that the crystallization process and phase transition of hard spheres in such system happens via heterogeneous nucleation.

5 2D versus 3D Freezing of a Lennard-Jones Fluid in a Slit Pore

In this chapter we present a computer simulation study of a (6,12)-Lennard-Jones fluid confined to a slit pore, formed by two uniform planes. These interact via a (3,9)-Lennard-Jones potential with the fluid particles. When the fluid approaches the liquid-to-solid transition, layering parallel to the walls is observed. In order to investigate the nature of the freezing transition, we performed a detailed analysis of the bond-orientational order parameter in the layers. We found no signs of hexatic order which would indicate a melting scenario of the Kosterlitz-Thouless type. An analysis of the mean-square displacement shows that the particles can easily move between the layers, making the crystallization a 3d-like process. This is consistent with the fact that we observe a considerable hysteresis in the heating-freezing curves, showing that the crystallization transition proceeds as an activated process.

with N. Gribova, A. Axel and C. Holm

5.1 Introduction and background

Understanding the structure and dynamics of confined fluids is important for processes such as wetting, coating, and nucleation. The properties of a fluid confined in a pore differ significantly from the bulk fluid due to finite size effects, surface forces and reduced dimensionality. The Lennard-Jones (LJ) model is one of the simplest models to study classical fluids and is interesting because it reproduces the thermodynamic behavior of simple fluids. This potential is an important model for exploring the behavior of simple fluids and has been used to study homogeneous vapor-liquid, liquid-liquid and liquid-solid equilibrium, melting and freezing [81, 82, 83, 84, 85, 86] and homogeneous and heterogeneous nucleation [87, 35, 88, 89, 90, 91]. It has also been used as a reference fluid for complex systems like colloidal and polymeric systems [92, 93].

The vapor-to-liquid transition in confined systems has been studied intensively, and it is well understood [94]. In the liquid phase, confinement to a slit induces layering at the walls. One could imagine this effect to facilitate crystallisation. And indeed it is known that depending on the strength of the particle-wall interaction the freezing scenario changes significantly [95, 96]. If the walls are strongly attractive, crystallisation starts from the walls and at a temperature higher than a situation without confinement. If the walls are strongly repulsive, crystallisation starts from the bulk at a temperature lower than without confinement. A well-distinguished layer of particles close to the wall can also, to some extent, be treated as a 2d system. This suggests that the freezing of such a layer proceeds via the Kosterlitz-Thouless-Halperin-Nelson-Young (KTHNY) mechanism [97, 98, 99, 100], meaning that the liquid turns into a crystal going through a hexatic phase [78].

This question has been studied by Radhakristan and coworkers [101] for a ratio of wall-particle to particle-particle attraction varying between 0 and 2.14. The pores were either 3 or 7.5 fluid particle diameters wide. For the narrower slit pore it was shown that around the freezing temperature the system exhibits a hexatic phase. With increasing wall attraction this temperature region becomes wider, i. e. an attractive wall facilitates the formation of the hexatic phase. The phase diagram for the wider pore with diameter 7.5 is more complicated. When the wall-particle attraction becomes bigger than the particle-particle attraction, at first a hexatic phase and then a crystal phase appear, however, only in the contact layers near the walls; the rest of the system remains liquid. Only when decreasing the temperature further the system crystallises completely. The temperature ranges, in which hexatic or crystal phases are observed only in the contact layers, again widens with growing wall-particle attraction. This indicates that the wall-particle attraction facilitates the formation of a hexatic phase even in wider pores, however only in the layers close to the walls. The same group of authors also reported that in a pore which can accommodate only a single layer

the KTHNY transitions are of second order, while already in a pore wide enough to accommodate two layers, they become first order transitions [101].

The type of frozen phases was studied by Vishnyakov and Neimark [102] depending on the size of the slit for this system. The distance between the walls was gradually increased up to a slit accommodating three layers. Depending on the width of the pore, hexagonal or orthorhombic phases were observed in the layers. They also reported that the diffusion coefficient in the hexatic phase is almost a magnitude smaller than in the liquid phase. In a study by Page and Sear freezing controlled by a pre-freezing in a similar system was also investigated [103]. Nucleation of the bulk crystal is affected by the surface phase behaviour. With increasing wall attraction, the bulk nucleation is smoothly transformed into nucleation of a surface crystal layer.

In this work we will discuss the liquid-to-solid transition in a slit pore and the process of the development of the solid phase. Here we investigate an attractive pore that is significantly wider, namely 20 diameters of a fluid particle. Studying the bond-orientational order parameter within the layers we observe no sign of a hexatic phase. An analysis of the mean-square displacement shows that the particles diffuse between the layers. Hence, the crystallization proceeds as a 3d process, as is also suggested by the noticeable hysteresis loop in the heating-freezing curve.

The chapter is structured as follows. In section 5.2 we describe our simulation method, and in section 5.3 we present the results at first for one value of the particle-wall interaction as a detailed example, followed by the generalisation to several other values and a discussion in section 5.4. We conclude with a summary of the presented results.

5.2 Simulation method

To study crystallization of confined colloidal system in a slit pore, we performed molecular dynamics (MD) simulations [104, 63] in the isothermal ensemble (NVT), i. e. the number of particles N , the volume V and the temperature T were fixed. The particles interact via the LJ-potential

$$u(r) = 4\epsilon \left[\left(\frac{\sigma}{r} \right)^{12} - \left(\frac{\sigma}{r} \right)^6 \right] \quad (5.1)$$

where r is the distance between the particles, σ the particle diameter and ϵ the depth of the minimum of the potential. The interaction between walls and particles is characterized by a LJ-potential integrated over semi-space:

$$u_w(r) = 4\epsilon \left[\left(\frac{\sigma}{r} \right)^9 - \left(\frac{\sigma}{r} \right)^3 \right]. \quad (5.2)$$

The particle-particle interaction was cut off at a distance $r_c = 2.5\sigma$ and the wall-particle interaction at a distance $r_c = 4.0\sigma$ (the wall-particle potential is wider and deeper than the particle-particle potential). Using the Steele potential [105] or just a (4,10)-LJ potential for the wall-particles interaction does not influence the results qualitatively. For the following we will use ϵ as the unit of energy, σ as the unit of length and $\tau = \sqrt{1 \cdot \sigma^2 / \epsilon}$ as unit of time (i.e. use the particle mass as the unit of mass); consequently, temperatures are given in multiples of $\epsilon/k_B T$.

The simulations were performed in a cubic box with periodic boundary conditions in the x - and y - directions and two walls positioned at $z = 0$ and $z = L_z = 20.45$. The other two dimensions of the simulation box were fixed as $L_x = L_y = 20.45$. The number of particles $N = 7768$ was chosen such that the density was kept constant at one particle per unit cube independent of the width of the slit. We used standard Nosé-Hoover thermostats to keep the temperature constant [106, 107, 108]. For the Nosé-Hoover thermostat, we set the effective mass $M_s = 0.5$. We simulated a cooling curve starting out from a random configuration at $T = 3.0$ and a melting curve starting out from a face-centered-cubic configuration at $T = 1.0$. Far away from the transition, the temperature was changed by $\Delta T = 0.1$ from one simulation run to the next, while close to transition we used a smaller increment/decrement, $\Delta T = 0.01$.

The simulations were implemented with a timestep of $\Delta t = 0.005$ and were let run for 1.0×10^6 MD steps for equilibration and for 2.5×10^5 for sampling. In order to compute the mean square displacement of the particles, a smaller timestep $\Delta t = 0.002$ was chosen, and to avoid influence of thermostat on the dynamics of the system we switched to the NVE ensemble after equilibration (keeping the total energy of the system E constant). We monitored the temperature, which fluctuated around a mean value practically equal to the temperature T in the NVT ensemble. Pressures were obtained from the virial expansion [109] omitting corrections for the cut-off in the potential.

5.3 Results and discussion

In this section, we present the results of liquid-solid transition of LJ colloidal particles confined in a slit pore. Figure 5.1 shows the pressure-temperature curves for heating and cooling curves. There is a considerable hysteresis, which indicates that the system has to overcome a free energy barrier when transforming from one phase to the other. Several runs were implemented both for heating and for cooling. The cooling lines coincide, whereas the temperature at which the melting process starts fluctuates. In Figure 5.1 we show the outer borders of the hysteresis region. As our system has attractive walls, crystallization should start from the walls [95]. This can be clearly seen in the snapshot (Figure 5.2) that was taken 90 MD steps after equilibration had

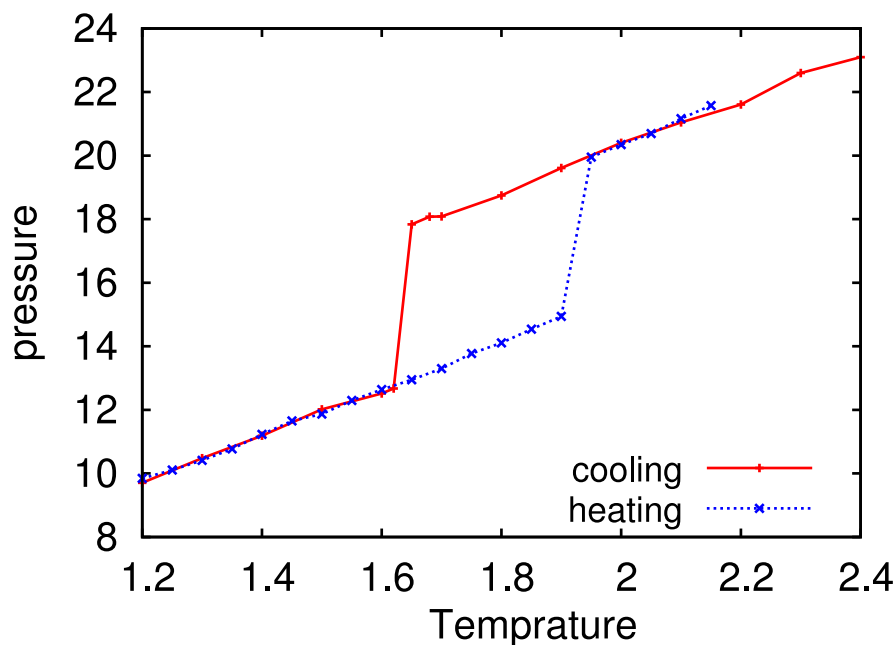


Figure 5.1: Pressure-Temperature curves for heating and cooling of a LJ-fluid confined between two uniform LJ(9,3)-walls. The outer borders of hysteresis are shown.

started. Only another 90 MD steps later the system completely crystallized. One can also see that no crystallization process has started at the top wall yet, demonstrating that this event is an activated process. As it was shown in [95] the width of hysteresis depends on the distance between the layers. If the distance differs considerably from the lattice constant of an ideal LJ crystal (0.916), the hysteresis will be more pronounced. For our system the distance is 0.87 in the bulk, and correspondingly the hysteresis is quite wide.

In order to investigate the phase transformation process, we now turn to the effects the walls have on the structure of the fluid. Figure 5.3 shows number density profiles $\varrho(z)$ for $L_z = 20.0\sigma$ in the liquid and the solid phase. In the liquid phase, the maxima of the peaks follow an exponential law $A[\exp(-Bx) + \exp(-(L_z - x)B)] + \rho_{\text{mid}}$, where ρ_{mid} is the density in the middle of the box. Figure 5.4 shows the behavior of the coefficient B with temperature. It can be seen that the values of B decrease more or less linearly at first, i. e. the number of layers increases and they become more pronounced. As soon as we enter the regime of the hysteresis at $T = 2.0$, B becomes almost constant (within the error of the simulations). This shows that the structure of the density profile does not change, no new layers appear and the system is trapped in the under-cooled state. As the liquid forms layers, one could assume that the transformation proceeds inside the layers via a KTHNY transition. In order to test this assumption, we now

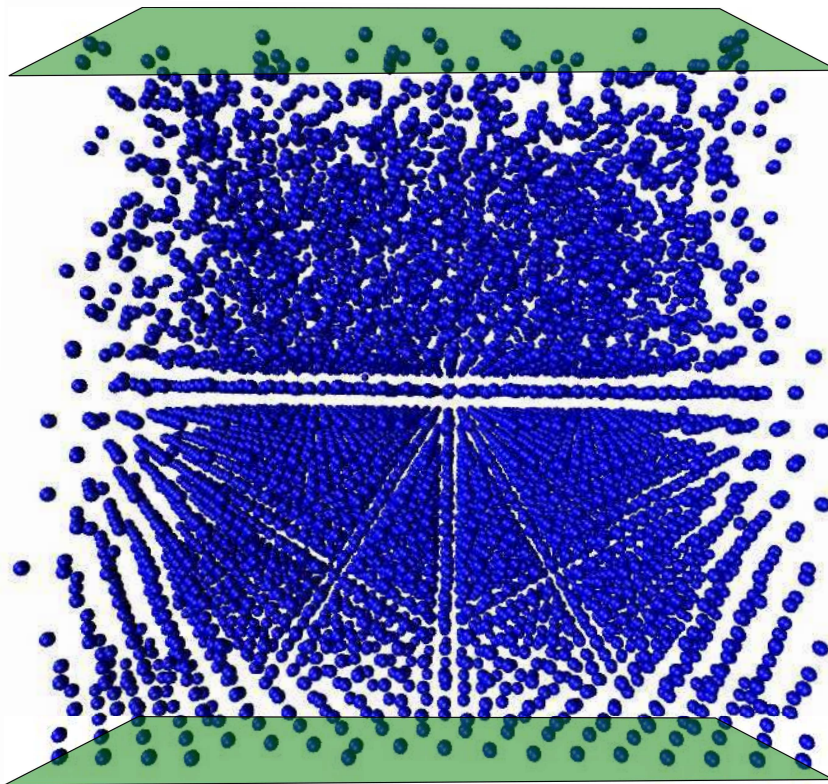


Figure 5.2: Snapshot of the system in the early stage of crystallization *at* $T = 1.60$. In this specific example it crystallizes from the bottom wall. The part on the bottom is already a crystal while the top side is still disordered.

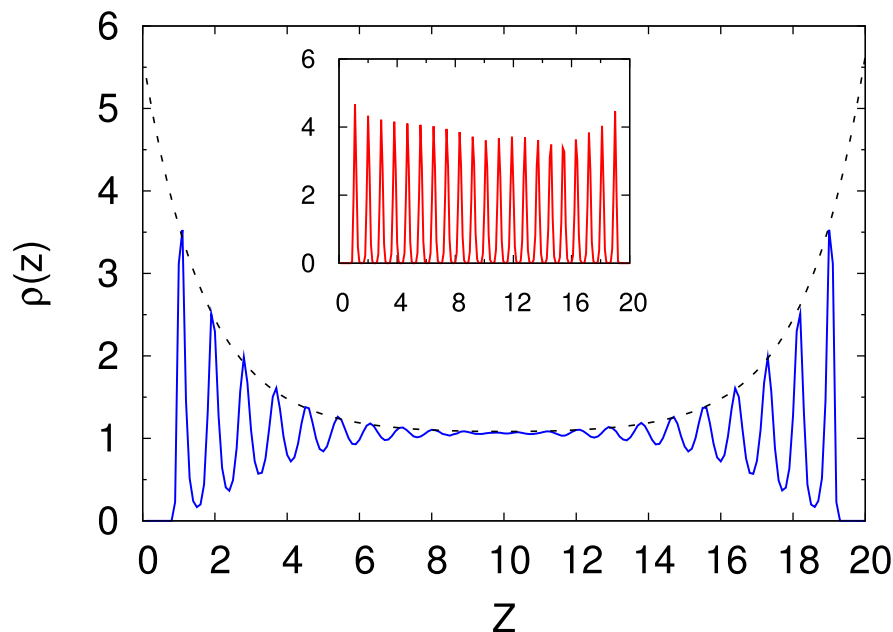


Figure 5.3: Density profile $\rho(z)$ of the liquid phase at $T = 1.70$. The heights of the peaks are fitted by an exponential function. The inset shows $\rho(z)$ for the solid phase at $T = 1.60$.

turn to the structure within the layers: To characterize the transitional order in one layer in 2D, we calculate the pair correlation (radial distribution) function:

$$g(r) = \rho^{-2} \left\langle \sum_{i, i \neq j} \delta(\mathbf{r}_i) \delta(\mathbf{r}_j - \mathbf{r}) \right\rangle \quad (5.3)$$

where ρ is the number density of particles in each layer. In Figure 5.5 the 2D radial distribution functions for the first and third layer (seen from the wall), the bulk part of the liquid and the first three layers of the solid phase are shown. The structure within the layers of the liquid becomes less pronounced as we move further away from the walls and is barely visible in the center of the box. Next we consider the bond-orientational order [78]: we define the local bond-orientational order parameter of particle j in layer m at a position \mathbf{x}_j as

$$\psi_6^m(\mathbf{x}_j) = \frac{1}{N_j} \sum_{k=1}^{N_j} e^{i6\theta_{jk}} \quad (5.4)$$

where N_j is the number of neighbors of particle j within layer m , the sum is over the neighbors k of j within m , and θ_{jk} is the angle between an arbitrary fixed axis and the line connecting particles j and k . The order of the m -th layer Ψ_6^m is defined as the

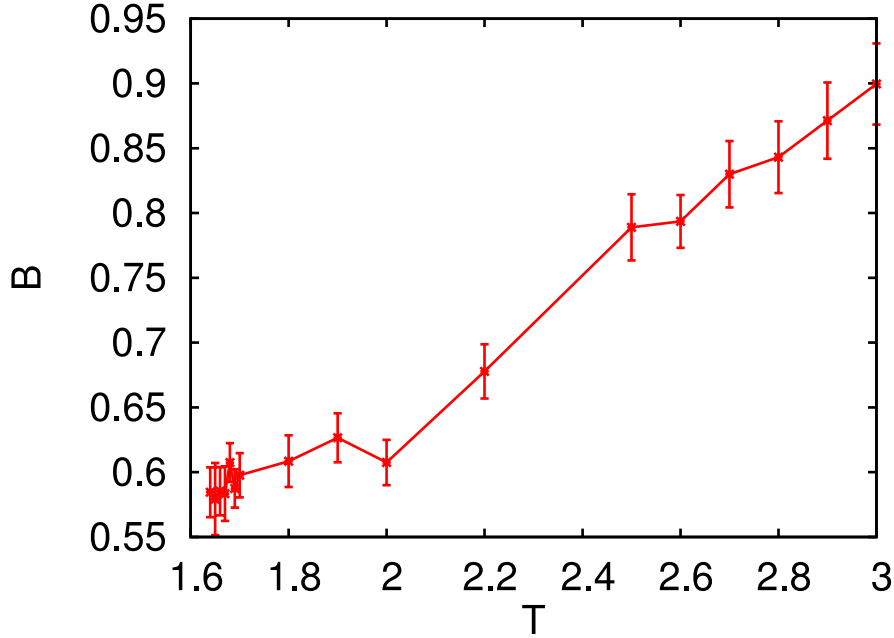


Figure 5.4: Coefficient B characterizing the exponential decay of density profile. In the hysteresis region ($T \leq 2.0$) it is almost not changing, i. e. the structure of the density profile stays the same.

average over $\psi_6^m(\mathbf{x}_j)$ for all N_m particles within the layer

$$\Psi_6^m = \frac{1}{N_m} \left| \sum_{j=1}^{N_m} \psi_6^m(\mathbf{x}_j) \right| \quad . \quad (5.5)$$

Figure 5.6 shows Ψ_6^m for various temperatures. When approaching the transition, the bond-orientational order close to the wall increases. The temperature dependence of Ψ_6^1 for the first layer of particles at the wall is shown in Figure 5.7. It clearly “jumps” i. e. is discontinuous at the transition. If the crystallization proceeded purely within the two-dimensional layers, one would observe a hexatic phase, which is characterized by a power-law decay of the correlation of the bond-orientational order

$$g_6(r) = \langle \psi_6^*(\mathbf{x}') \psi_6(\mathbf{x}' - \mathbf{x}) \rangle \quad , \quad (5.6)$$

where the average is taken over all particles within a layer whose positions \mathbf{x} are a distance r apart. Figure 5.8 shows $g_6(r)$ for the first layer at $T = 1.67$ and $T = 1.66$. The system jumps from the 2d-liquid phase into the 2d-solid without visiting a hexatic phase first. Hence the crystallization process is not of the KTHNY-kind. To find out why the crystallization process is 3d-like despite the layering, we now consider the particle’s dynamics. One of the obvious characteristics is to estimate how long

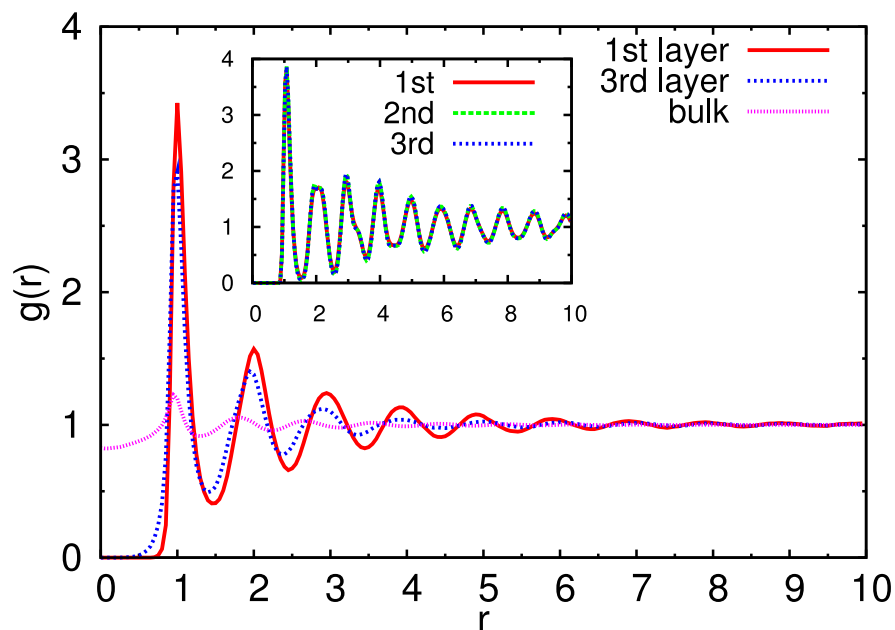


Figure 5.5: 2D pair correlation function in the first and third layer and the bulk part of the system in the liquid state at $T = 1.65$. The inset shows $g(r)$ for the first three layers at the wall for the solid state at $T = 1.60$

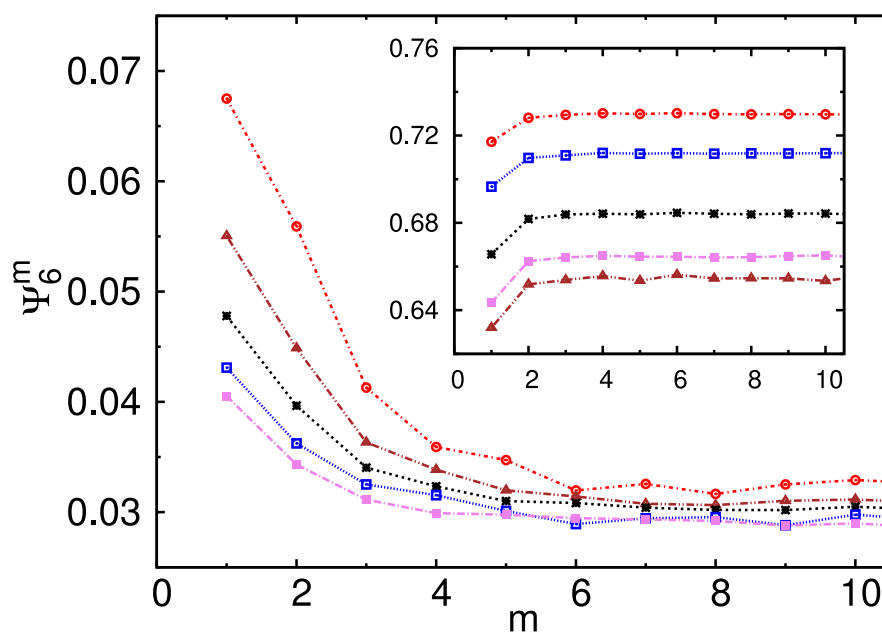


Figure 5.6: 2D bond-orientation order parameter Ψ_6^m for liquid states depending on the layer m for temperatures 1.70, 1.80, 2.00, 2.20, 2.40 (from top to bottom). The inset shows Ψ_6^m for solid states for temperatures 0.80, 1.00, 1.30, 1.50, 1.60 (from top to bottom).

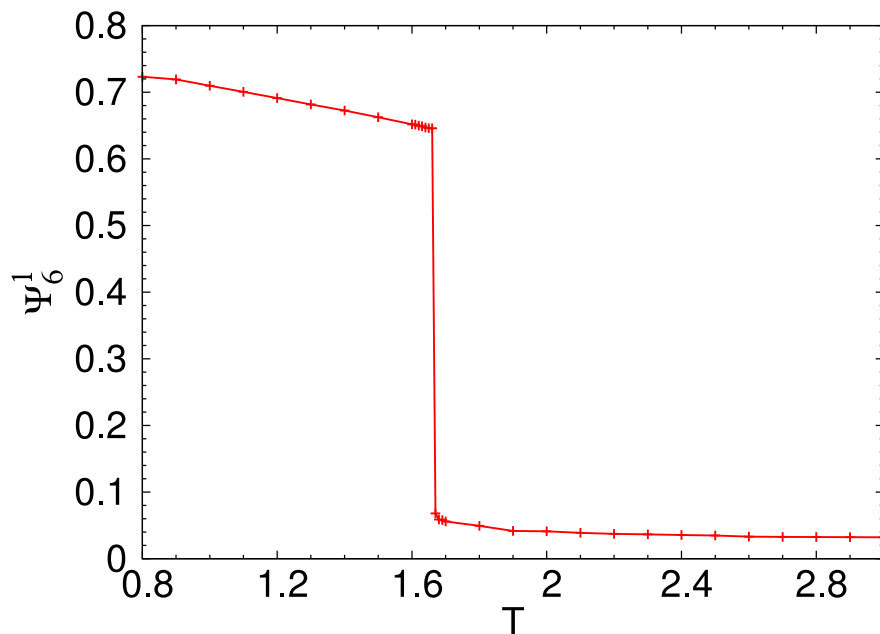


Figure 5.7: 2D bond-orientation order parameter Ψ_6^1 of the first layer from the wall as a function of the temperature.

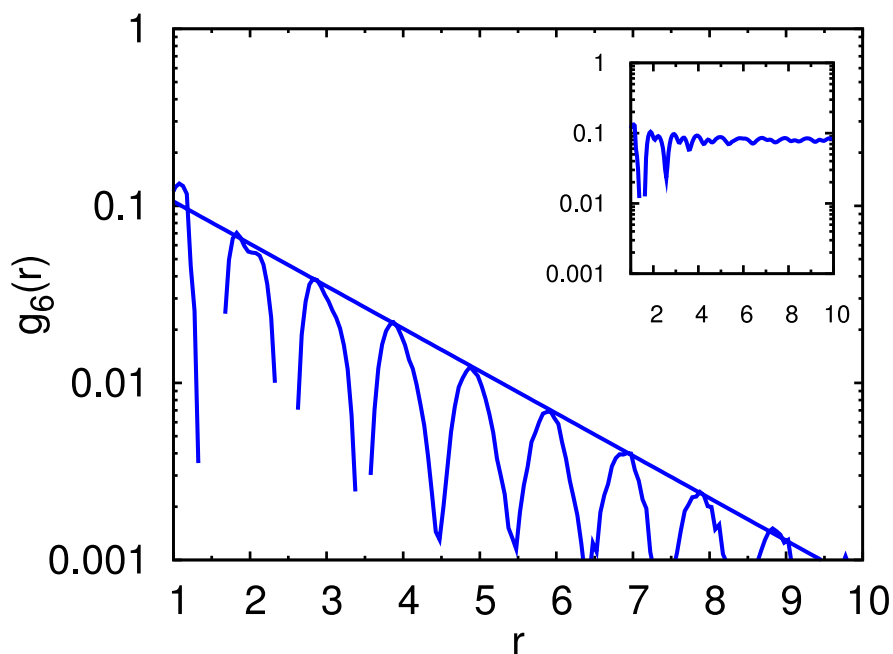


Figure 5.8: Bond-orientational correlation function for the liquid state just before freezing at $T = 1.67$ for the layer closest to the wall. The solid line is the result of an exponential fit. There is no signature of a hexatic phase. The inset shows g_6 for the crystalline state at the next available lower temperature $T = 1.66$, right after the transition.

particles on average stay in the layer closest to the wall. The easiest way to estimate this is to calculate how many particles of those which were in the layer at time 0 remained there at the time t . From Figure 5.9 we can see that the ratio of particles that remain in the layer decreases exponentially with time. Fitting it with $\exp(-t/\tau)$ we obtain the average lifetime τ of a particle in the layer (Figure 5.10). It increases linearly with the decrease of temperature and is then fluctuating around the mean value in the hysteresis region. As we observed already for the density, the behavior of the system in the hysteresis region does not change much during cooling. To characterize

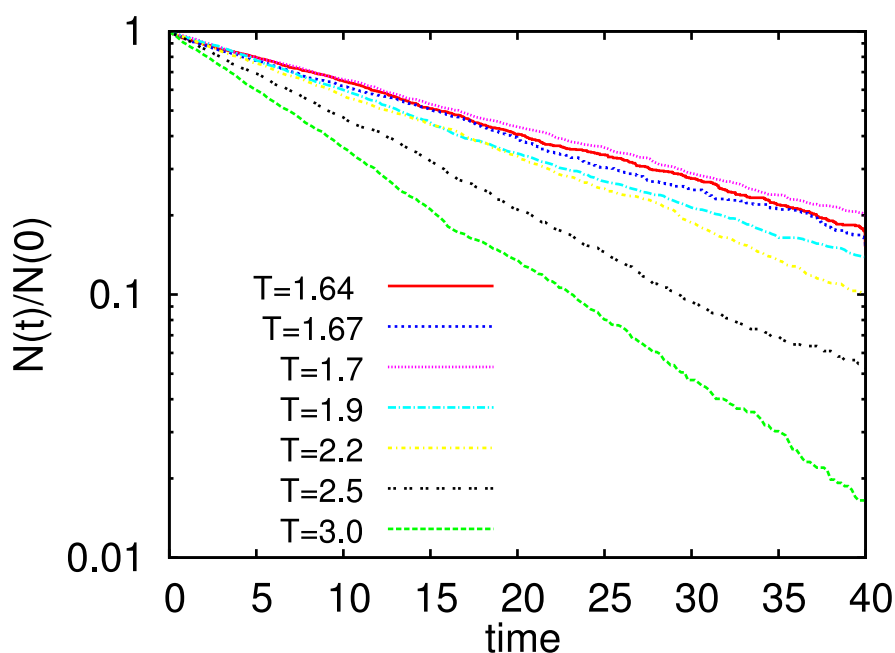


Figure 5.9: Ratio of particles in the layer closest to the wall that stayed there from time 0 ($N(0)$) until time t ($N(t)$) at different temperatures above the phase transition.

the mobility of the particles we calculated the mean square displacement (MSD). As the system forms layers, we calculate the MSD parallel and perpendicular to the wall separately. Looking at the plane parallel to the wall (Figure 5.11) while approaching crystallization, we observe that the particles in the layer closest to the wall are a little faster than the particles in the bulk, despite the fact that the crystallization typically starts from here. We take this as another hint that the crystallization proceeds as a 3d-process, and does not first start within the layer closest to the wall. The behavior of the particles does not change significantly on approach of the crystallization as they enter the metastable region. The mean square displacement measured perpendicular to the wall (Figure 5.11) shows that after the ballistic regime for a while particles are trapped in the layer and then start leaving it. It is not meaningful to calculate the

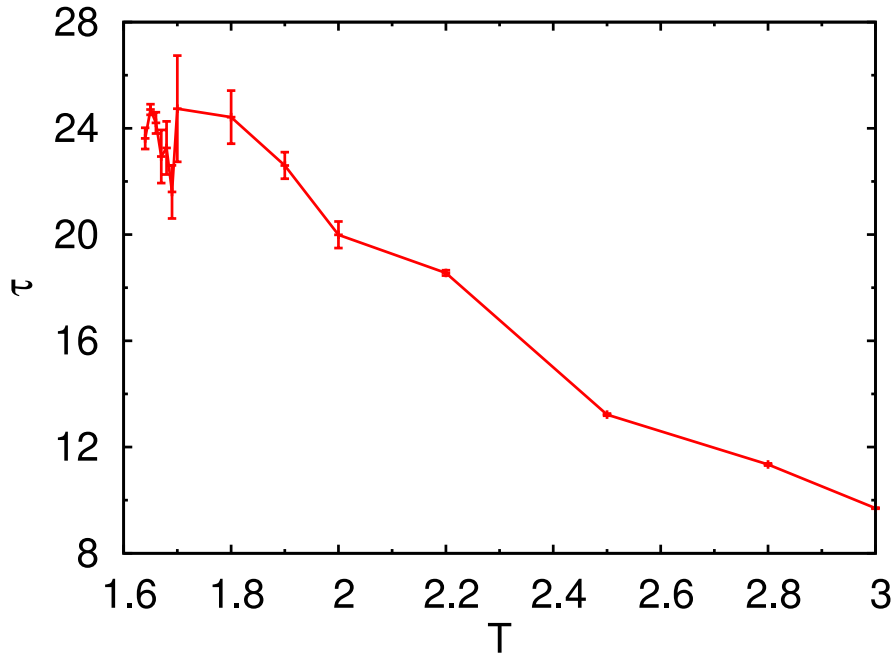


Figure 5.10: Average lifetime of particles in the utmost layer as a function of temperature. In the hysteresis region the lifetime does not change significantly.

diffusion coefficient in our system, because the particles do not stay long enough in a layer for the MSD to enter the linear regime.

5.4 Conclusion

We reported on a molecular dynamics study of the liquid-to-solid transformation of a LJ fluid in a wide slit pore. Although the confinement induces layering in the liquid phase close to the walls, we do not find a successive, layerwise crystallization. Crystallization is still a 3d process, and, in particular, no hexatic phase was observed in the layers closest to the wall, excluding the possibility of a 2D KTHNY-like crystallization within the layers; in fact, the mobility of particles in the layers is higher than their mobility in the bulk. Nevertheless, we find that crystallization in the system practically always starts from the walls, i. e., the walls facilitate crystallization. And although crystallization is an activated process similar to 3d crystallization, we observe a smaller hysteresis, indicating a reduced nucleation barrier as compared to bulk crystallization.

Altogether, our simulations suggest that the nucleation of the LJ fluid close to a planar wall does not significantly differ from the nucleation in the bulk, although with a smaller nucleation barrier. This can however be easily understood as an effect of the strongly increased density in the layers close to the confinement.

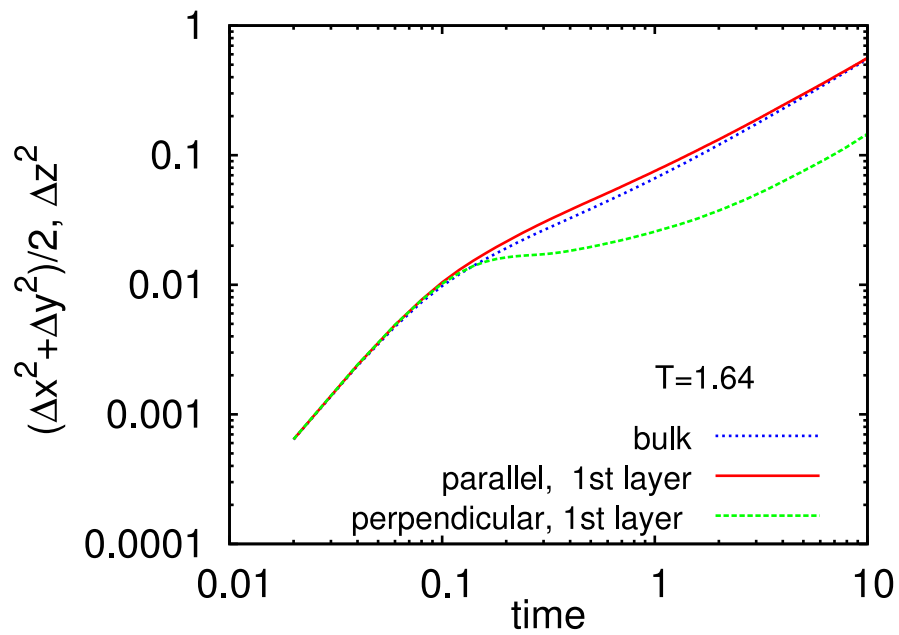


Figure 5.11: Mean square displacement for $T = 1.64$. The MSD parallel to the wall is almost identical in the layer and in the bulk with the particles in the layer even being slightly faster. The MSD perpendicular to the wall show a clear trapping effect.

6 Summary and outlook

Let us summarize the most important results presented in this dissertation. In the thesis, considering Monte Carlo simulation [62, 63], homogeneous and heterogeneous crystal nucleation in hard sphere systems have been studied. We used forward flux sampling (FFS) technique [5, 6, 7] combining with local bond-order parameter analysis [36, 37] for distinction of liquid- and solid-like particles and also identification of the largest crystalline cluster. By these combinations, we predicted crystal nucleation rates and also analyzed the feature of pathways in the phase space. We also applied conventional molecular dynamic simulation method [104, 63] to study crystallization of Lennard-Jones colloidal particles confined between two planar wall.

In the first step, we studied homogeneous crystal nucleation in hard spheres. Simulations are done for different degrees of supersaturation in the moderate supercooling. Brute force MC simulations showed that, it is difficult to observe spontaneous nucleation for given pressures. we found a swell agreement in nucleation rates between our results and umbrella sampling simulation results of Ref [13] for mono-disperse and 5% polydisperse colloidal particles. Next we compare FFS results with experimental data and also brute force molecular dynamic and Monte Carlo simulations. Similar to results of the umbrella sampling, the discrepancy between numerical results and experimental data for the low degree of under-cooling (low value in volume friction) is exist and let us also add that we have still not found an intuitive physical explanation and origin of the discrepancy between our results with experimental data in low supersaturation. Furthermore, we computed the critical Gibbs free-energy barrier and compared our results with US results and also classical nucleation theory predictions. We found an acceptable agreement between FFS data for free energies and data for classical nucleation theory. Finally we analyzed crystalline clusters in the system by computing gyration tensor components. These analysis indicate that for the small size of nuclei, clusters are more elongated. However, by increasing number of particles in largest clusters, crystalline clusters become more compact and with ellipsoidal forms.

Next, we reported on numerical study of the effect of bcc (100) structured hard wall on the heterogeneous crystal nucleation and crystallization of hard sphere colloids. Comparing to the bulk system, presence of the wall lowers the Gibbs free energy barrier and the range of metastability becomes narrow. We systematically explored how structure affects the ability of the wall to induce crystallization and 2D analysis

for the layers close to different wall structures point out that bcc (100) structure is suggestible to study heterogeneous nucleation. Then we predicted the nucleation rates for the moderate degrees of supersaturation near and above coexistence bulk pressure. These predictions are first numerical results for such systems. Then we analyzed the crystalline clusters and pathways by computing the gyration tensor. Our observation indicate that largest crystals take place via the creation, formation and growth of a compact crystalline cluster at the wall. Also we used radius of gyration components to predict a rough estimation of the contact angles. For different supersaturations, The value of contact angles show that the crystallization of hard sphere colloids at bcc (100) structured wall is occur via heterogeneous nucleation and the system is far from wetting region.

Finally, we examined the conventional molecular dynamics study of the liquid-solid transformation of a Lennard-Jones system in a slit pore. We performed the system in constant temperature and constant volume (NVT) ensemble. For such system we performed two dimensional analysis by using local bond order parameter in $2d$ [78] and found that crystallization in such system is still a $3d$ process, and it can be an advisable system to study heterogeneous nucleation in LJ colloidal systems. $2d$ analysis shows that in particular, no hexatic phase can be observed in the layers closest to the wall, excluding the possibility of a 2D KTHNY-like crystallization within the layers. Nevertheless, we find that crystallization in the system practically always starts from the walls, i. e., the walls facilitate crystallization. And although crystallization is an activated process similar to 3d crystallization, we observe a smaller hysteresis, indicating a reduced nucleation barrier as compared to bulk crystallization.

List of Figures

1.1	Schematic snapshots of a cluster	2
2.1	P-V and F-V schematic diagrams	7
2.2	Two examples of homogeneous and heterogeneous nucleation	9
2.3	Schematic formation of nucleus in the metastable phase	9
2.4	CNT prediction of Gibbs free-energy	12
2.5	Phase space in FFS scheme	18
2.6	Forward flux sampling procedure	19
2.7	A particle and its neighbors	22
2.8	q_6 distribution function	23
2.9	$\mathbf{q}_6(i) \cdot \mathbf{q}_6(j)$ probability distribution function	24
2.10	Probability distribution of connected particles	24
3.1	Equation of state of bulk hard sphere system	28
3.2	Brute force MC results of the Gibbs free-energy	29
3.3	Snapshot of a hard sphere system	31
3.4	FFS results of $P(n)$ in homogeneous nucleation	33
3.5	Density of different systems in different pathways	34
3.6	Homogeneous nucleation rates	35
3.7	Mean square displacement for the bulk hard sphere system	36
3.8	The height of Gibbs free energy barrier	37
3.9	Typical Snapshots of critical nucleus	38
3.10	Radius of gyration of clusters in the bulk system	39
3.11	Average radius of gyration for the bulk system	40
4.1	Density profile of the confined hard sphere liquid	44
4.2	Snapshot of a hard sphere system confined between two walls	45
4.3	2D bond orientation order parameter	47
4.4	Probability of reaching cluster size n in heterogeneous nucleation	48
4.5	Snapshots of critical clusters at the structured wall	49
4.6	A typical snapshot of heterogeneous nucleation process	50
4.7	Radius of gyration of clusters at the structured wall	51
4.8	Radius of gyration in homogeneous and heterogeneous nucleation	51

4.9	Contact angle of crystalline clusters at the structured wall	52
5.1	Pressure-Temperature curves for LJ system	59
5.2	Snapshot of the LJ system confined between two planar walls	60
5.3	Density profile of the liquid and the solid LJ colloids	61
5.4	Exponential decay of density profile in the liquid state	62
5.5	2D pair correlation function	63
5.6	2D bond-orientation order parameter in different layers	63
5.7	2D bond-orientation order parameter as a function of temperature . . .	64
5.8	Bond-orientational correlation function	64
5.9	lifetime of particles in the layer	65
5.10	Average lifetime of particles	66
5.11	MSD parallel and perpendicular to the planar wall	67

List of Tables

3.1	Computational details used in FFS simulation runs	30
3.2	FFS simulation results of homogeneous crystal nucleation	32
4.1	Details of FFS used in heterogeneous nucleation simulations	47
4.2	FFS results of the prediction of heterogeneous nucleation rates	47

Bibliography

- [1] D. B. Fahrenheit. *Phil. Trans. Roy. Soc.*, 39:78, 1724.
- [2] D. Turnbull and J. C. Fisher. *J. Phys. Chem.*, 17:71, 1949.
- [3] J. W. Gibbs. *Trans. Connect. Acad.*, 3:108, 1878.
- [4] M. Volmer and A. Weber. *Z. Phys. Chem.*, 119:227, 1926.
- [5] R. J. Allen, P. B. Warren, and P. Rein ten Wolde. Sampling rare switching events in biochemical networks. *Phys. Rev. Lett.*, 94(1):018104, 2005.
- [6] R. J. Allen, D. Frenkel, and P. Rein ten Wolde. Simulating rare events in equilibrium or nonequilibrium stochastic systems. *J. Chem. Phys.*, 124(2):024102, 2006.
- [7] R. J. Allen, D. Frenkel, and P. Rein ten Wolde. Forward flux sampling-type schemes for simulating rare events: Efficiency analysis. *J. Chem. Phys.*, 124(19):194111, 2006.
- [8] R. J. Allen, C. Valeriani, and P. Rein ten Wolde. Forward flux sampling for rare event simulations. *J. Phys.: Condens. Matter*, 21(46):463102, 2009.
- [9] F. A. Escobedo, E. E. Borrero, and J. C. Araque. Transition path sampling and forward flux sampling. applications to biological systems. *J. Phys.: Condens. Matter*, 21(33):333101, 2009.
- [10] G. M. Torrie and J. P. Valleau. Monte carlo free energy estimates using non-Boltzmann sampling: Application to the sub-critical Lennard-Jones fluid. *Chem. Phys. Lett.*, 28(4):578–581, 1974.
- [11] G. M. Torrie and J. P. Valleau. Nonphysical sampling distributions in monte carlo free-energy estimation: Umbrella sampling. *J. Comput. Phys.*, 23(2):187–199, 1977.
- [12] J. S. van Duijneveldt and D. Frenkel. Computer simulation study of free energy barriers in crystal nucleation. *J. Chem. Phys.*, 96(6):4655, 1992.

-
- [13] S. Auer and D. Frenkel. Prediction of absolute crystal-nucleation rate in hard-sphere colloids. *Nature*, 409(6823):1020–1023, 2001.
- [14] L. Filion, M. Hermes, R. Ni, and M. Dijkstra. Crystal nucleation of hard spheres using molecular dynamics, umbrella sampling, and forward flux sampling: A comparison of simulation techniques. *J. Chem. Phys.*, 133(24):244115, 2010.
- [15] T. Schilling, S. Dorosz, H. J. Schöpe, and G. Opletal. Crystallization in suspensions of hard spheres: a monte carlo and molecular dynamics simulation study. *J. Phys.: Condens. Matter*, 23(19):194120, 2011.
- [16] J. L. Harland and W. van Megen. Crystallization kinetics of suspensions of hard colloidal spheres. *Phys. Rev. E*, 55(3):3054, 1997.
- [17] A. Stipp C. Sinn, A. Heymann and T. Palberg. *Prog. Colloid Polym. Sci.*, 118:266, 2001.
- [18] K. Schtzel and B. J. Ackerson. Density fluctuations during crystallization of colloids. *Phys. Rev. E*, 48(5):3766, 1993.
- [19] P. M. Chaikin and T. C. Lubensky. *principles of Condensed Matter Physics*. Cambridge University Press, Cambridge, 1995.
- [20] L. Farkas. *Z. Phys. Chem.*, 125:236, 1927.
- [21] R. Becker and W. Döring. *Ann. Phys.*, 24:719, 1935.
- [22] J. L. Katz. Homogeneous nucleation theory and experiment: A survey. *Pure and Appl. Chem.*, 64(11):1661–1666, 1992.
- [23] D. Oxtoy. *J. Phys.: Condens. Matter*, 4:7627, 1992.
- [24] J. Zeldovich. *J. Exp. Theo. Phys. (Russia)*, 12:525, 1942.
- [25] J. B. Anderson. Statistical theories of chemical reactions. distributions in the transition region. *J. Chem. Phys.*, 58(10):4684, 1973.
- [26] D. Chandler. Statistical mechanics of isomerization dynamics in liquids and the transition state approximation. *J. Chem. Phys.*, 68(6):2959, 1978.
- [27] C. Dellago, P. G. Bolhuis, F. S. Csajka, and D. Chandler. Transition path sampling and the calculation of rate constants. *J. Chem. Phys.*, 108(5):1964, 1998.
- [28] P. G. Bolhuis, C. Dellago, and D. Chandler. Reaction coordinates of biomolecular isomerization. *Proc. Natl. Acad. Sci.*, 97(11):5877 –5882, 2000.

-
- [29] P. G. Bolhuis, D. Chandler, C. Dellago, and Ph. L. Geissler. TRANSITION PATH SAMPLING: throwing ropes over rough mountain passes, in the dark. *Annu. Rev. Phys. Chem.*, 53(1):291–318, 2002.
- [30] T. S. van Erp, D. Moroni, and P. G. Bolhuis. A novel path sampling method for the calculation of rate constants. *J. Chem. Phys.*, 118(17):7762, 2003.
- [31] T. S. van Erp and P. G. Bolhuis. Elaborating transition interface sampling methods. *J. Comput. Phys.*, 205(1):157–181, 2005.
- [32] D. Moroni, T. S. van Erp, and P. G. Bolhuis. Investigating rare events by transition interface sampling. *Physica A*, 340(1-3):395–401, 2004.
- [33] D. Moroni, P. G. Bolhuis, and T. S. van Erp. Rate constants for diffusive processes by partial path sampling. *J. Chem. Phys.*, 120(9):4055, 2004.
- [34] D. Moroni, T. S. van Erp, and P. G. Bolhuis. Simultaneous computation of free energies and kinetics of rare events. *Phys. Rev. E*, 71(5):056709, 2005.
- [35] D. Moroni, P. R. ten Wolde, and P. G. Bolhuis. Interplay between structure and size in a critical crystal nucleus. *Phys. Rev. Lett.*, 94(23):235703, 2005.
- [36] P. J. Steinhardt, D. R. Nelson, and M. Ronchetti. Bond-orientational order in liquids and glasses. *Phys. Rev. B*, 28(2):784, 1983.
- [37] P-R ten Wolde, M. J. Ruiz-Montero, and D. Frenkel. Numerical evidence for bcc ordering at the surface of a critical fcc nucleus. *Phys. Rev. Lett.*, 75(14):2714, 1995.
- [38] P.R ten Wolde, M. J. Ruiz-Montero, and D. Frenkel. Simulation of homogeneous crystal nucleation close to coexistence. *Faraday Discuss.*, 104:93, 1996.
- [39] H. K. Christenson. Confinement effects on freezing and melting. *J. Phys.: Condens. Matter*, 13:R95, 2001.
- [40] P. N. Pusey and W. van Megen. Phase behaviour of concentrated suspensions of nearly hard colloidal spheres. *Nature*, 320(6060):340–342, March 1986.
- [41] W. G. Hoover and F. H. Ree. Melting transition and communal entropy for hard spheres. *J. Chem. Phys.*, 49(8):3609, 1968.
- [42] U. Gasser. Crystallization in three- and two-dimensional colloidal suspensions. *J. Phys.: Condens. Matter*, 21(20):203101, 2009.

-
- [43] D. Frenkel and A. J. C. Ladd. New monte carlo method to compute the free energy of arbitrary solids. application to the fcc and hcp phases of hard spheres. *J. Chem. Phys.*, 81(7):3188, 1984.
- [44] J. M. Polson and D. Frenkel. Calculation of solid-fluid phase equilibria for systems of chain molecules. *J. Chem. Phys.*, 109(1):318, 1998.
- [45] N. B. Wilding and A. D. Bruce. Freezing by monte carlo phase switch. *Phys. Rev. Lett.*, 85(24):5138, 2000.
- [46] T. Zykova-Timan, J. Horbach, and K. Binder. Monte carlo simulations of the solid-liquid transition in hard spheres and colloid-polymer mixtures. *J. Chem. Phys.*, 133(1):014705, 2010.
- [47] M. Amini and B. B. Laird. Kinetic coefficient for Hard-Sphere crystal growth from the melt. *Phys. Rev. Lett.*, 97(21):216102, 2006.
- [48] R. L. Davidchack and B. B. Laird. Direct calculation of the Hard-Sphere crystal /Melt interfacial free energy. *Phys. Rev. Lett.*, 85(22):4751, 2000.
- [49] R. L. Davidchack, J. R. Morris, and B. B. Laird. The anisotropic hard-sphere crystal-melt interfacial free energy from fluctuations. *J. Chem. Phys.*, 125(9):094710, 2006.
- [50] T. Zykova-Timan, R. E. Rozas, J. Horbach, and K. Binder. Computer simulation studies of finite-size broadening of solidliquid interfaces: from hard spheres to nickel. *J. Phys.: Condens. Matter*, 21(46):464102, 2009.
- [51] D. W. Marr and A. P. Gast. Interfacial free energy between Hard-Sphere solids and fluids. *Langmuir*, 10(5):1348–1350, 1994.
- [52] S. Auer and D. Frenkel. Suppression of crystal nucleation in polydisperse colloids due to increase of the surface free energy. *Nature*, 413(6857):711–713, 2001.
- [53] B. O'Malley and I. Snook. Crystal nucleation in the hard sphere system. *Phys. Rev. Lett.*, 90(8):085702, 2003.
- [54] T. Schilling, H. J. Schpe, M. Oettel, G. Opletal, and I. Snook. Precursor-Mediated crystallization process in suspensions of hard spheres. *Phys. Rev. Lett.*, 105(2):025701, 2010.
- [55] A. Cacciuto, S. Auer, and D. Frenkel. Onset of heterogeneous crystal nucleation in colloidal suspensions. *Nature*, 428(6981):404–406, 2004.

- [56] S. Auer and D. Frenkel. Line tension controls Wall-Induced crystal nucleation in Hard-Sphere colloids. *Phys. Rev. Lett.*, 91(1):015703, 2003.
- [57] D. Winter, P. Virnau, and K. Binder. Monte carlo test of the classical theory for heterogeneous nucleation barriers. *Phys. Rev. Letters*, 103(22):225703, 2009.
- [58] U. Gasser, E. R. Weeks, A. Schofield, P. N. Pusey, and D. A. Weitz. Real-Space imaging of nucleation and growth in colloidal crystallization. *Science*, 292(5515):258–262, 2001.
- [59] R. P. A. Dullens, D. L. Aarts, and W. K. Kegel. Dynamic broadening of the Crystal-Fluid interface of colloidal hard spheres. *Phys. Rev. Lett.*, 97(22):228301, 2006.
- [60] I. B. Ramsteiner, K. E. Jensen, D. A. Weitz, and F. Spaepen. Experimental observation of the crystallization of hard-sphere colloidal particles by sedimentation onto flat and patterned surfaces. *Phys. Rev. E*, 79(1):011403, 2009.
- [61] J. Hernández-Guzmán and E. R. Weeks. The equilibrium intrinsic crystalliquid interface of colloids. *Proc. Natl. Acad. Sci.*, 106(36):15198–15202, 2009.
- [62] P. D. Landau and k. Binder. *A Guide to Monte Carlo Simulation in Statistical Physics*. Cambridge University Press, Cambridge, 1969.
- [63] D. Frenkel and B. Smit. *Understanding Molecular Simulation*. Academic Press, 2002.
- [64] Z J. Wang, C. Valeriani, and D. Frenkel. Homogeneous bubble nucleation driven by local hot spots: A molecular dynamics study. *J. Phys. Chem. B*, 113(12):3776–3784, 2009.
- [65] J. A. van Meel, A. J. Page, R. P. Sear, and D. Frenkel. Two-step vapor-crystal nucleation close below triple point. *J. Chem. Phys.*, 129(20):204505, 2008.
- [66] M. Fasolo and P. Sollich. Fractionation effects in phase equilibria of polydisperse hard-sphere colloids. *Phys. Rev. E*, 70(4):041410, October 2004.
- [67] P. N. Pusey, E. Zaccarelli, C. Valeriani, E. Sanz, Wilson C. K. Poon, and Michael E. Cates. Hard spheres: crystallization and glass formation. *Philosophical Transactions of the Royal Society A: Mathematical, Physical and Engineering Sciences*, 367(1909):4993 –5011, December 2009.
- [68] R. P. Sear. Nucleation: theory and applications to protein solutions and colloidal suspensions. *J. Phys.: Condens. Matter*, 19(3):033101, 2007.

-
- [69] P. G. Debenedetti. *metastable liquids*. Princeton University Press, Princeton, 1996.
- [70] A. C. Zettlemoyer. *Nucleation*. M. Dekker, New York, 2005.
- [71] D. Turnbull. Kinetics of heterogeneous nucleation. *J. Chem. Phys.*, 18(2):198, 1950.
- [72] N. H. Fletcher. Size effect in heterogeneous nucleation. *J. Chem. Phys.*, 29(3):572, 1958.
- [73] M. Dijkstra. Capillary freezing or complete wetting of hard spheres in a planar hard slit? *Phys. Rev. Lett.*, 93(10):108303, 2004.
- [74] E. Mendez-Villuendas and R. K. Bowles. Surface nucleation in the freezing of gold nanoparticles. *Phys. Rev. Lett.*, 98(18):185503, 2007.
- [75] M. Heni and H. Loewen. Surface freezing on patterned substrates. *Phys. Rev. Lett.*, 85:3668, 2000.
- [76] A. Cacciuto and D. Frenkel. Simulation of colloidal crystallization on finite structured templates. *Phys. Rev. E*, 72(4):041604, 2005.
- [77] W. S. Xu, Z. Y. Sun, and L. J. An. Heterogeneous crystallization of hard spheres on patterned substrates. *J. Chem. Phys.*, 132(14):144506, 2010.
- [78] K. J. Strandburg. Two-dimensional melting. *Rev. Mod. Phys.*, 60(1):161, 1988.
- [79] V. K. Shen and P. G. Debenedetti. A computational study of homogeneous liquidvapor nucleation in the Lennard-Jones fluid. *J. Chem. Phys.*, 111(8):3581, 1999.
- [80] D. Winter, P. Virnau, and K. Binder. Heterogeneous nucleation at a wall near a wetting transition: a monte carlo test of the classical theory. *J. Phys.: Condens. Matter*, 21(46):464118, 2009.
- [81] L. Verlet. Computer "Experiments" on classical fluids. i. thermodynamical properties of Lennard-Jones molecules. *Phys. Rev.*, 159(1):98, 1967.
- [82] J. P. Hansen and L. Verlet. Phase transitions of the Lennard-Jones system. *Phys. Rev.*, 184(1):151, 1969.
- [83] K. Singer, A. Taylor, and J. V. L. Singer. Thermodynamic and structural properties of liquids modelled by 2-Lennard-Jones centres pair potentials. *Mol. Phys.*, 33(6):1757, 1977.

-
- [84] J. J. Nicolas, K. E. Gubbins, W. B. Streett, and D. J. Tildesley. Equation of state for the Lennard-Jones fluid. *Mol. Phys.*, 37(5):1429, 1979.
- [85] J. D. Honeycutt and H. C. Andersen. Molecular dynamics study of melting and freezing of small Lennard-Jones clusters. *J. Phys. Chem.*, 91(19):4950–4963, 1987.
- [86] J. K. Johnson, J. A. Zollweg, and K. E. Gubbins. The Lennard-Jones equation of state revisited. *Mol. Phys.*, 78(3):591, 1993.
- [87] P. R. ten Wolde and D. Frenkel. Computer simulation study of gasliquid nucleation in a Lennard-Jones system. *J. Chem. Phys.*, 109(22):9901, 1998.
- [88] X. M. Bai and M. Li. Calculation of solid-liquid interfacial free energy: A classical nucleation theory based approach. *J. Chem. Phys.*, 124(12):124707, 2006.
- [89] L. J. Peng, J. R. Morris, and Y. C. Lo. Temperature-dependent mechanisms of homogeneous crystal nucleation in quenched Lennard-Jones liquids: Molecular dynamics simulations. *Phys. Rev. B*, 78(1), 2008.
- [90] H. Wang, H. Gould, and W. Klein. Homogeneous and heterogeneous nucleation of Lennard-Jones liquids. *Phys. Rev. E*, 76(3):031604, 2007.
- [91] F. Trudu, D. Donadio, and M. Parrinello. Freezing of a Lennard-Jones fluid: From nucleation to spinodal regime. *Phys. Rev. Lett.*, 97(10):105701, 2006.
- [92] A. Baumgartner. Statics and dynamics of the freely jointed polymer chain with Lennard-Jones interaction. *J. Phys. Chem.*, 72(2):871, 1980.
- [93] O. Guzman and J. J. de Pablo. An effective-colloid pair potential for Lennard-Jones colloidpolymer mixtures. *J. Phys. Chem.*, 118(5):2392, 2003.
- [94] L. D. Gelb, K. E. Gubbins, R. Radhakrishnan, and M. Sliwinska-Bartkowiak. Phase separation in confined systems. *Rep. Progr. Phys.*, 62(12):1573–1659, 1999.
- [95] M. Miyahara and K. E. Gubbins. Freezing/melting phenomena for Lennard-Jones methane in slit pores: A monte carlo study. *J. Chem. Phys.*, 106(7):2865, 1997.
- [96] C. Alba-Simionesco, B. Coasne, G. Dosseh, G. Dudziak, K. E. Gubbins, R. Radhakrishnan, and M. Sliwinska-Bartkowiak. Effects of confinement on freezing and melting. *J. Phys.: Condens. Matter*, 18(6):R15–R68, 2006.
- [97] J. M. Kosterlitz and D. J. Thouless. Ordering, metastability and phase transitions in two-dimensional systems. *J. Phys. C: Solid State Phys.*, 6(7):1181–1203, 1973.
- [98] B. I. Halperin and D. R. Nelson. Theory of Two-Dimensional melting. *Phys. Rev. Lett.*, 41(2):121, 1978.

-
- [99] D. R. Nelson and B. I. Halperin. Dislocation-mediated melting in two dimensions. *Phys. Rev. B*, 19(5):2457, 1979.
- [100] A. P. Young. Melting and the vector coulomb gas in two dimensions. *Phys. Rev. B*, 19(4):1855, 1979.
- [101] R. Radhakrishnan, K. E. Gubbins, and M. Sliwinska-Bartkowiak. Global phase diagrams for freezing in porous media. *J. Chem. Phys.*, 116(3):1147, 2002.
- [102] A. Vishnyakov and A. V. Neimark. Specifics of freezing of Lennard-Jones fluid confined to molecularly thin layers. *J. Chem. Phys.*, 118(16):7585, 2003.
- [103] A. J. Page and R. P. Sear. Freezing in the bulk controlled by prefreezing at a surface. *Phys. Rev. E*, 80(3):031605, 2009.
- [104] M. P. Allen and D. J. Tildesley. *Computer Simulation of Liquids*. Clarendon, Oxford, 1987.
- [105] W. A. Steele. The physical interaction of gases with crystalline solids: I. gas-solid energies and properties of isolated adsorbed atoms. *Surf. Sci.*, 36(1):317–352, 1973.
- [106] S. Nose. A unified formulation of the constant temperature molecular dynamics methods. *J. Chem. Phys.*, 81(1):511, 1984.
- [107] S. Nose. A molecular dynamics method for simulations in the canonical ensemble. *Mol. Phys.*, 52(2):255, 1984.
- [108] W. G. Hoover. Canonical dynamics: Equilibrium phase-space distributions. *Phys. Rev. A*, 31(3):1695, 1985.
- [109] J. P. Hansen and I. R. McDonald. *Theory of Simple Liquids*. Academic Press, London, 1986.



Hamed Maleki

CONTACT INFORMATION

Condensed Matter Theory Group (Komet 331),
Institute of Physics, Johannes Gutenberg-University,
Staudinger weg 7,
55099 Mainz,
Germany

Tel: +49 6131 39 25158
Mobile: +49 176 64 241 221
Fax: +49 6131 39 25441
E-mail: maleki@uni-mainz.de

PERSONAL DETAILS

gender:	male
Date of birth:	June, 10, 1982
Place of birth:	Birjand, Iran
Citizenship:	Iranian
Marital Status:	Married

EDUCATION

Ph.D. student, Condensed Matter Physics, Johannes Gutenberg-University, Mainz, Germany,

- Thesis Topic: *Heterogeneous nucleation of colloidal suspension in hard sphere and Lennard-Jones models*
- Supervisor: Prof. Dr. Tanja Schilling
- Adviser: Prof. Dr. Friederike Schmid

M.Sc., Condensed Matter Physics, University of Birjand, Birjand, Iran, July 2007

- Thesis Topic: *Granular materials in quasi two dimensional (Hele- Shaw) cell.*
- Supervisor: Prof. Dr. Fatemeh Ebrahimi
- Adviser: Prof. Dr. Ehsan Nedaaee Oskoei (IASBS, Zanjan, Iran)

B.Sc., Applied Physics, University of Birjand, Birjand, Iran, July 2004

- Thesis Topic: *Non-equilibrium statistical mechanics (transport properties) of simple liquids*
- Supervisor: Prof. Dr. Behzad Haghghi

PUBLICATION

Thesis:

- Ph. D. Thesis: *Numerical study of homogeneous and heterogeneous crystal nucleation in colloidal system*, To be submitted in May 2011.
- M. Sc. Thesis: *Phase diagrams for bi-dispersed granular media in Hele- Shaw cell.*, July 2007(In Persian).
- B. Sc. Thesis: *Perturbation theory in non-equilibrium statistical mechanics of simple liquids*, Jun 2005 (In Persian).

Journal:

- B. Haghighi, H. Maleki, S.J. Shakhs Emampour, "Non-equilibrium ensemble method: A quantum-statistical-mechanical approach", *Indian J. Pure Appl. Phys.*, **44**, (2006), pp. 378-384.
- H. Maleki, F. Ebrahimi, E. Nedaaee Oskoe, "The angle of repose of spherical grains in granular Hele-Shaw cells: a molecular dynamics study", *J. Stat. Mech.: Theory Exp.* 2008, P04026.
- H. Maleki, F. Ebrahimi, A. Amirabadizadeh, "Phase diagram of bi-dispersed granular materials in vertical Hele-Shaw cell", unpublished.
- F. Ebrahimi, T. Azizpour, H. Maleki, "Janssen effect and the stability of quasi-two-dimensional sandpile", *Phys. Rev. E* **82**, 031302 (2010).
- S. J. Shakhs Emampour, B. Haghighi, H. Maleki, "Non-Equilibrium Statistical Thermodynamic Perturbation Theory: A General approach to Maxwellian Molecules", *Indian J. Pure Appl. Phys.*, **49**, (2011), pp. 199-203.
- H. Maleki and P. E. Theodorakis, "Structure of bottle-brush brushes under good solvent conditions. A molecular dynamics study, unpublished.
- N. Gribova, A. Arnold, H. Maleki, T. Schilling, C. Holm, "2D versus 3D Freezing of a Lennard-Jones Fluid in a Slit Pore", unpublished.
- H. Maleki, et al. *Structured wall effect on rate of heterogeneous nucleation of hard sphere colloidal system: A Monte Carlo simulation*, In preparation for submission.